Design and Fabrication of Functional Scaffolds for Bone Regeneration Applications

Rabeil Sakina

NUST201260460MSMME62412F

SUPERVISOR

Dr. Murtaza Najabat Ali

CO-SUPERVISOR

Dr. Mushtaq Khan

Department of Biomedical Engineering and Sciences
School of Mechanical and Manufacturing Engineering
National University of Sciences and Technology
2015

Declaration

It is hereby declared that this research study has been conducted for the partial fulfillment of requirements for the degree of Master of Science in Biomedical Sciences. I hereby declare that no portion of this work has been submitted in support of an application for another degree to any other university. All the work done during the course of this study is original and work based on other studies has been cited accordingly.

Rabeil Sakina

Form TH – 4: Master's Thesis Work

We hereby recommend that the dissertation prepared under our supervision by **Rabeil Sakina (NUST201260453MSMME62312F)**, titled**: Design and Fabrication of Functional Scaffolds for Bone Regeneration Applications** be accepted in partial fulfillment of the requirements for the award of **MS** degree with ___ Grade.

Examination Committee Members

Dr. Muhammad Nabeel Anwar _____

Dr. Umer Ansari _____

Dr. Syed Husain Imran _____

Co-Supervisor

Dr. Mushtaq Khan _____

Supervisor

Dr. Murtaza Najabat Ali _____

_____

Dr. Muhammad Nabeel Anwar
Head of Department
Biomedical Engineering and Sciences

_____

Principal/Dean
School of Mechanical and Manufacturing Engineering
National University of Sciences and Technology
Islamabad, Pakistan

This work is dedicated to my parents who have always been proud of me, at my best and even more at my worst. Thank you for your unwavering faith in me.

To my brother Qarib Hasnain, whose admiration for me motivates me to do better every day.

To my sister Noreen Akhter, because some bonds are thicker than blood.

To my grandparents, for sharing their stories with me which I shall cherish forever.

Acknowledgement

I would like to acknowledge the efforts of Dr. Murtaza Najabat Ali and Dr. Mushtaq Khan for the completion of my project. I would like to thank them for their valuable advice and guidance throughout the duration of this project.

I would also like to thank Dr. Muhammad Nabeel Anwar for his advice and constant support. Thank you for always finding the time to listen to my grievances, no matter how insignificant. I would also like to acknowledge Dr. Nouman ul Haq for help with obtaining results.

Finally, I would like to thank Zahra Fazal and Samran Navid for their friendship, advice, criticism and encouragement, all of which have been invaluable to me these past two years.

Rabeil Sakina

Table of Contents

List of Figures

List of Tables

List of Abbreviations

Poly (vinyl alcohol)	----------	PVA
Polyurethane	----------	PUR
Extracellular Matrix	----------	ECM
Poly (lactic acid)	----------	PLA
Poly (glycolic acid)	----------	PGA
Poly (ε-caprolactone)	----------	PCL
Critical Size Defect	----------	CSD
Thermally Induced Phase Separation	----------	TIPS
Computer Aided Design	----------	CAD
Computer Numerical Control	----------	CNC
Scanning Electron Microscope	----------	SEM
Universal Testing Machine	----------	UTM
Young's Modulus of Compression	----------	E
Stress	----------	σ
Strain	----------	ϵ
Phosphate Buffer Saline	----------	PBS
Fourier Transform Infrared Spectroscopy	----------	FTIR
Hydroxyapatite	----------	HA
Frequency of Vibration	----------	v

ABSTRACT

Bone tissue regeneration across critical sized segmental bone defects requires external intervention in order to enable tissue growth across the gap which would otherwise be non-regenerating. Such intervention commonly includes use of bone grafts which have inherent limitations. In this research, a synthetic scaffold device was fabricated using the polymer poly (vinyl alcohol) (PVA) and an attachment mechanism was designed for the device for use in long bone fractures. Electrospinning was used in order to fabricate scaffold with porosity at the micro scale which is an essential feature for cellular integration. The scaffolds were augmented with sheets fabricated using mold casting in order to enhance the mechanical strength of the device. The final device was fabricated with electrospun and casted specimen stacked in an alternating manner. A hollow, tubular sleeve was fabricated using polyurethane (PUR) and used for the attachment mechanism. The device was cut into the shape of a disc of 20 mm diameter and inserted into the polymeric sleeve. Specimen of the device having dimension 20 x 20 x 6 mm for length, width and height respectively were used for analysis using scanning electron microscope, universal testing machine and phosphate buffer saline for studying scaffold morphology, device strength and degradation rate respectively. The results showed that PVA electropsun mats had nanofiber diameter of 87.42 ± 38.53 nm and pore size of 0.5 μm. Mechanical strength of the device under compressive loading yielded compressive strength of 0.49 ± 0.07 MPa while degradation rate of the scaffold was 270 minutes. A 3-D scaffold was hence fabricated in this study that can enable both functional and mechanical properties to be achieved using two relatively simple fabrication techniques.

Keywords: bone tissue engineering, scaffold, 3-D, load bearing, electrospinning, mold casting, poly (vinyl alcohol) (PVA)

CHAPTER ONE

Introduction

1. Tissue Engineering and Regenerative Medicine

The field of tissue engineering deals with applications that aim to repair and/or replace damaged or failing body tissue and organs. Tissue engineering involves principles of both engineering and life sciences in order to develop suitable synthetic alternatives in order to restore, maintain or improve tissue or whole organ function (1).

2. Bone Tissue Engineering

Bone tissue defects can be due to accidents or the aging population and are commonly encountered in clinical scenarios. These segmental bone defects are a cause of concern in cases where a critical size defect occurs such that bone tissue is unable to repair across the gap on its own. Such non-unions require a bridge that acts as a conducting medium for bone regeneration across the gap (1)(2).

Current treatment options for critical size bone tissue defects are the use of bone grafts including autografts and allografts. Autografts, being from the patient's own bone, are the preferred mode of treatment for bone defects. They do not pose the risk of immune response from the patient, in addition to being osteoinductive and osteoconductive owing to the presence of growth factors, high vascularity and extracellular matrix (ECM) content and so are conducive to bone tissue growth (3). However, autografts are limited in the amount of graft material that can be extracted and may be inadequate in cases where the gap between the bone ends is too wide. Also, donor site morbidity is an issue since graft extraction requires an additional surgical procedure and hence may affect patient recovery (4).

Allografts are an alternative source of bone graft material and are often obtained from a cadaver. Such grafts have little or no cellular content and their properties may be catered for the host body requirements (5). Immune reactions, however, are a complication associated with their

use and there is a risk of infection transfer. They are also in frequent short supply and unable to meet growing demands (6).

Bone tissue engineering aims to provide synthetic alternatives to current treatment methods. These alternates to bone grafts may overcome limitations associated with their use such as immune response, shortage of supply and donor site complications (3).

Engineered constructs for bone tissue repair face several challenges before they become a viable treatment option for bone defects. The scaffold needs to be biocompatible and hence closely mimic the natural ECM of bone. There is also the matter of strength versus vascularity wherein the scaffold needs to have sufficient porosity to enable tissue and nutrients to easily move through it while also needing sufficient strength to withstand external pressures. There is normally a trade-off between these two features since high porosity may lead to compromise in mechanical strength while high mechanical strength may be the result of increased packing density which reduces the porosity of the scaffold.

3. Bone Physiology

Bone may be present in either woven or lamellar form. Woven bone is randomly organized collagen fibers that normally form during fetal bone development or bone fractures as a result of rapid osteoid formation by osteocytes. Remodeling over time replaces woven bone by lamellar bone which has an ordered structure due to parallel arrangement of collagen into sheets of lamellae (7).

Three main cell types can be found in bone namely osteoblasts, osteocytes and osteoclasts with each having different roles in bone formation and remodeling. Osteoblasts differentiate from mesenchymal stem cells and secrete osteoid, the non-collagenous proteins that form the bone matrix, as they mature. The osteoid matrix is responsible for mineralization of bone due to the presence of hydroxyapatite which confers hardness and rigidity to bone. Hydroxyapatite is the main inorganic constituent of bone (7).

Osteoblasts are responsible for the synthesis of the precursors of collagen I. Collagen I is the main organic constituent of bone matrix. Osteoblasts also secrete non-collagenous proteins such as osteocalcin and osteopontin (8); osteocalcin is the most abundant non-collagenous protein in bone matrix (7).

As they mature within the bone matrix, osteoblasts become osteocytes that remain trapped within the bone matrix secreted by the precursor osteoblasts. However, not all of them become osteoclasts. When bone reaches maturation, a majority of osteoblasts that do not form osteoclasts undergo apoptosis while the rest convert to bone-lining cells (9). These bone-lining cells are essential to bone repair since they can revert to osteoblast cells under stress conditions (10). Additionally, bone-lining cells regulate mineral content of bone ECM, hence their role in bone homeostasis (9).

Osteocytes are the most abundant cell type found in bone. Extensions of the plasma membranes of osteocytes enable them to communicate with each other and their environment. Subsequently, it may be that osteocytes act as mechanosensors for bone and so they may instruct osteoclasts and osteoblasts on when to resorb and form bone respectively (11).

4. Bone Anatomy

The bone functions as a dynamic system within the body that facilitates locomotion, protects vital organs of the body and plays part in maintaining homeostasis (12). The bone undergoes constant remodeling and responds to environmental stimuli. It is one of the few organ systems that can regenerate without leaving scar tissue (9). Bones can be categorized as long bones, short bones, flat bones and irregular bones. The long bone is typically organized into two main tissue types, the cortical and cancellous (trabecular) bone.

4.1 Cortical Bone

Cortical bone is the dense, compact outer bone that surrounds the inner marrow and provides mechanical strength to the bone. The basic functional unit of bone is known as an osteon. The cortical osteon (or haversian system) is a collection of cells and ECM organized in a concentric lamellar pattern that surrounds the haversian canal. The haversian canal enables vascularity within the cortical layer since it contains blood vessels and neurons. The cortical layer is surrounded by the periosteum which is abundant in osteoprogenitors such as osteoblasts and osteoclasts that play crucial role in repair mechanisms (9)(13).

4.2 Cancellous/Trabecular Bone

The cancellous or trabecular bone is the inner porous region of the bone and has a honeycombed appearance. The trabecular osteon are also called packets and are organized as concentric lamellae. The trabecular bone is a network of rods and plates that forms the bone marrow component of the bone (9).

4.3 Bone Membranes

The two membranes present in bone are the periosteum and the endosteum. The periosteum surrounds the outer cortical layer of the bone. It is supplied by blood vessels and nerve fibers and contains osteoblasts and osteoclasts that subsequently become involved in bone repair mechanisms when needed. The periosteum is fixed to the cortical layer by use of thick collagenous fibers that are embedded into the bone tissue (9).

The endosteum covers the inner surface of cortical and trabecular bone as well as the blood vessel canals present within the bone. This membrane is in contact with the bone marrow and also has a supply of blood vessels as well as osteoblasts and osteoclasts (9).

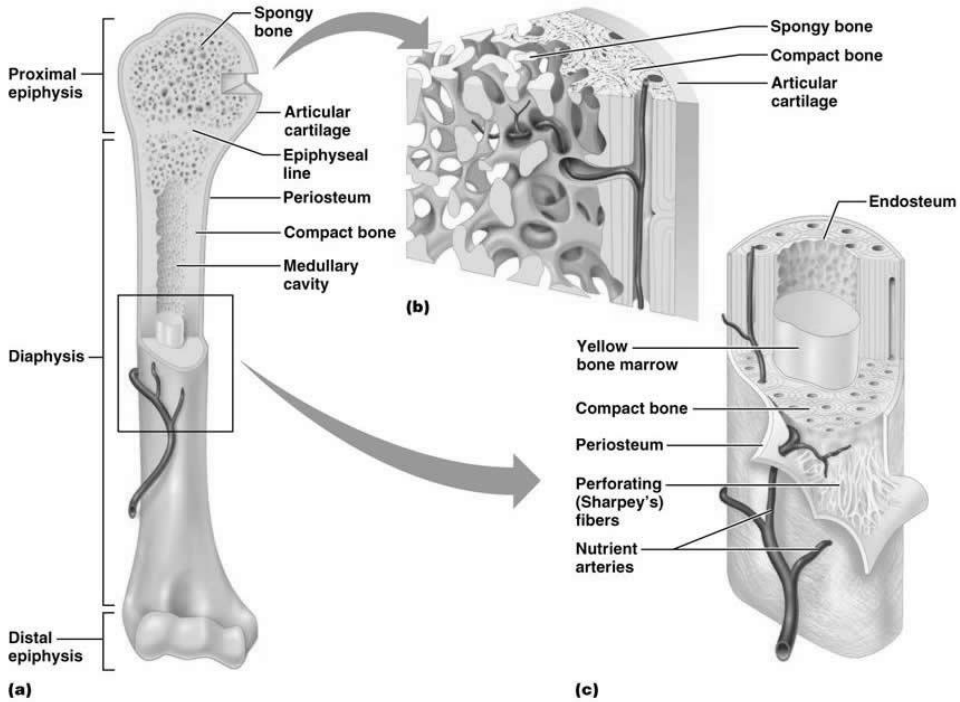

Figure 1: The figure shows (a) the typical anatomy of a long bone, (b) the structure of the epiphysis and (c) diaphysis (http://classes.midlandstech.edu/carterp/Courses/bio210/chap06/lecture1.html)

5. Bone Properties

Cortical bone has compression strength in the range of 130 to 180 MPa, tensile strength of 50 to 151 MPa and elastic modulus in the range of 12 to 18 GPa (14). On average, bone has compressive strength of 70-280 MPa and tensile strength 60-70 MPa.

6. Types of Biomaterials for Bone Tissue Engineering

In the past, where materials used for bone implant designs were focused on being inert, the focus has now shifted to use of materials that are bioactive in nature (15). Such biomaterials actively recruit cells from the surrounding tissue to the site of implant (15)(1). In the case of bone, biomaterials for tissue repair should ideally enable osteoinduction, osteoconduction and osseointegration (12). Osteoinductive biomaterials allow for recruitment of progenitor bone cells and promote their maturation to osteoblastic lineage. Osteoconduction is achieved by promoting bone growth into and across the cross-sectional area of the implant (12). Biomaterials capable of osseointegration enable stable anchorage of the implant via direct bone-to-implant contact (12).

6.1 Ceramics

Bioactive materials such as bioglass and ceramics provide surface modifications at the tissue-implant interface that enable bone tissue growth at the implant surface. Calcium phosphate ceramics in particular have been shown to have great osteoconductive and ostoinductive potential (16). Ceramics such as hydroxyapatite and calcium phosphates for the most part closely mimic natural bone mineral composition and hence, in addition to being biocompatible, support osteoblast differentiation in bone ECM (17)(18). Since hydroxyapatite is a stable component of bone ECM, its degradation in the physiological environment is slow. Subsequently, hydroxyapatite and calcium phosphate based implants show slow degradation rates over time due to their inertness in the body tissue, upto periods of several years (19). Since implants need degradation rates that correspond to tissue proliferation and healing rates, slow degradation over extended periods of time makes use of such ceramics less desirable. Analogues to hydroxyapatite such as amorphous hydroxyapatite and tricalcium phosphate have greater degradation rates but are not mechanically stable for porous scaffolds (16). In general, ceramics are brittle in nature and hence prone to failure in load bearing applications (12).

6.2 Polymers

Polymers used in scaffolds for bone tissue engineering can be either from natural-derived materials or synthetic polymers. Among natural-based polymers, collagen is perhaps the most widely used since it is part of the ECM of many major tissues such as bone, cartilage, tendon and muscle and so enable better osteointegration (12). It accounts for almost 30% of all proteins present in the body and confers strength and flexibility to the body tissue (20). Hence its use is highly desirable in fabricating scaffolds since it is biocompatible and elicits a low immunogenic response. Natural polymers such as alginate are used in cartilage regeneration due to their ability to induce chondrocyte proliferation (21). Hyaluronan is another natural-derived polymer that has potential for cartilage regeneration but has high degradation rate (22). Use of polymers from natural sources pose the risk of transmission of disease to the implant site and may also elicit immune response from the body (12).

The most commonly investigated synthetic polymers for bone tissue engineering include poly(lactic acid) (PLA), poly(glycolic acid) (PGA) and poly(ε-caprolactone) (PCL) . Synthetic polymers enable flexibility in processing parameters since they can be used in a wide range of manufacturing techniques for scaffold fabrication (12). In addition to being biocompatible, they are mechanically strong and hence more useful in load-bearing applications.

6.3 Composites

Composite materials enable the desirable properties of two or more materials to be combined into one functional material in order to meet the scaffold requirements. Most commonly, blends of polymers and ceramics are used to fabricate composite materials. Such composites combine the properties of polymer formability and, together with the ceramic phase, enable greater mechanical strength (23). Since polymers are not inherently bioactive, combination with ceramic materials confers bioactivity to the scaffold (24).

7. Scaffold Design for Bone Tissue

For three-dimensional scaffold design for bone tissue engineering, there are several factors that need to be taken into consideration. Scaffolds require optimum porosity in order to allow cellular mass to easily penetrate through the structure as well as to allow for the uptake of

nutrients and removal of waste from the structure. In this context, vascularization of the scaffold is an important design consideration. On average, the optimum pore size required for bone scaffolds is around 300μm (25) and a porosity of 90% or greater is desirable (26).

Bone scaffolds also require mechanical strength equal to or greater than that of normal bone in order to sustain mechanical loading and provide a stable structure for cellular proliferation and growth. The degradation rates of the scaffold should match bone tissue growth such that the structural integrity of the structure is not compromised. Interconnectivity between the pores of the scaffold is also desirable in order to provide even cellular distribution and to ensure adequate nutrient supply (27).

8. Scaffold Fabrication Techniques

Various fabrication techniques are used for building three-dimensional scaffolds for tissue engineering. These techniques include phase separation (28), self-assembly (29), electrospinning (30) and rapid prototyping (31). Phase separation is a relatively simple technique for fabricating 3-D scaffolds and can produce scaffolds with porosities in the range of microns. However, use of organic solvents in the preparation of these scaffolds leaves undesirable residues in the resulting structure (32). Also, scaffolds fabricated by phase separation are not mechanically strong for use in load bearing applications. Self-assembly allows for the development of an intricate 3D structure that closely mimics the natural ECM but produces scaffolds that are mechanically weak as well as time consuming in their fabrication (33). Rapid prototyping allows for scaffold fabrication in less time and allows for versatility in scaffold design but scaffold porosity is limited in this technique (30).

8.1 Electrospinning

The process of electrospinning is based on the principle of electrostatic induction and is used to produce fibers in the range of a few microns to several nanometers in diameter. The term electrospinning was coined from Anton Formhals' use of the term electrostatic spinning in 1934. Between 1964 and 1969, a mathematical model to describe the cone shaped structure formed by a droplet of fluid when placed under an electrostatic force was introduced. This was later called

the Taylor cone, a familiar characteristic form observed in liquid solutions placed under electrostatic charge in electrospinning (34).

The three major components of a typical electrospinning setup are a high voltage power supply, metallic spinneret and a grounded collector plate. Voltage from the high voltage power supply, when applied to a metallic spinneret causes the polymeric solution within the spinneret to become charged. The polymeric solution gains the same charge and, eventually, repulsion forces with the solution overcome surface tension and it ejects from the tip of the solution as a continuous jet stream. This stream is attracted by and travels towards the grounded collector plate.

After the jet stream has travelled a distance from the needle tip, the liquid loses electrical, surface and molecular stability, forming an expanding coil structure. Eventually, the solvent evaporates and leaves behind a solidified nanofiber which stretches and reduces in diameter to give a solid polymer fiber. This solidified fiber continues to travel towards the collector on which it is deposited as a mat of random or aligned nanofibers.

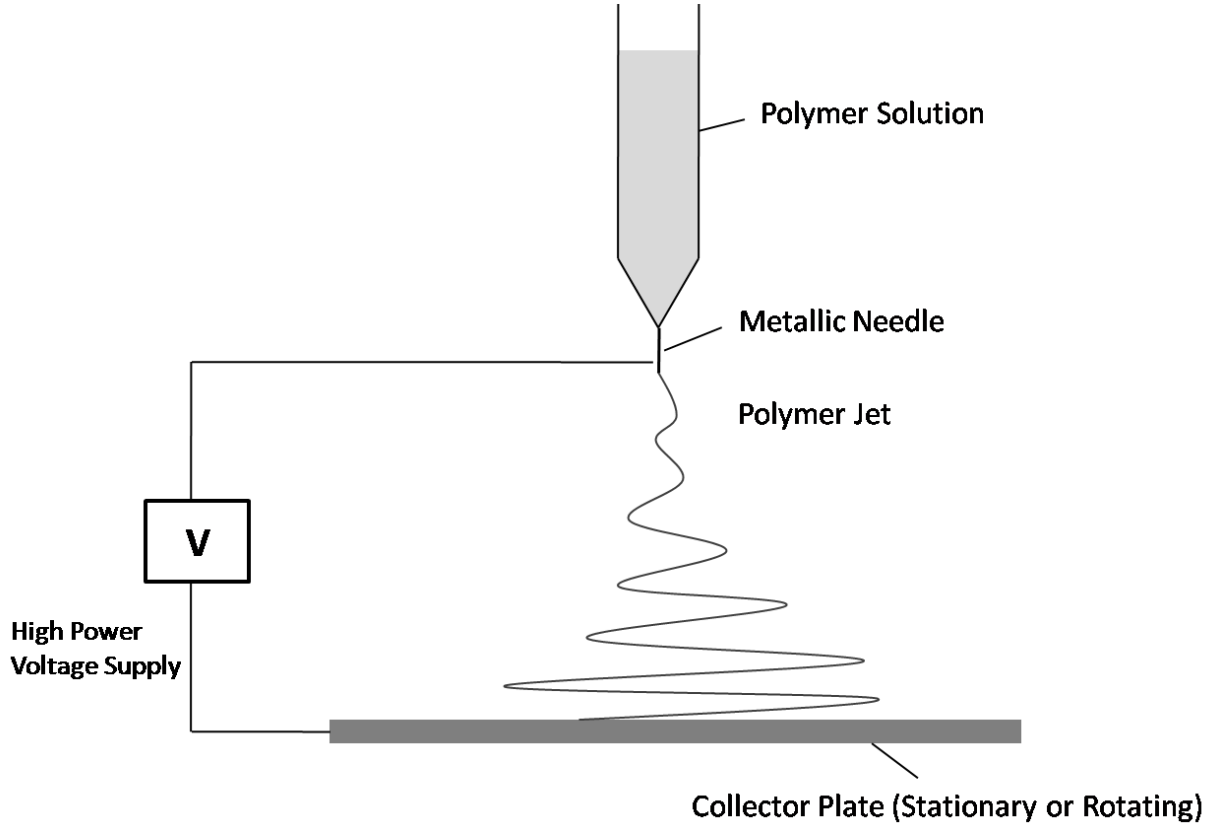

Figure 2: A typical electrospinning setup (Adapted from (35))

Electrospinning collector configurations can be modified in order to suit the scaffold requirements; plate and rotating mandrel are two typical collector types. Applied voltage, polymer concentration, distance of collector from tip of spinneret and polymer injection rate all affect nanofiber configuration and deposition.

8.2 Nanofiber Formation

When high voltage is applied to the polymer solution, the pendant drop at the tip of the spinneret needle becomes highly electrified. This induces charges that are evenly distributed throughout the polymer solution. Consequently, two types of electrostatic forces act upon the pendant drop. Electrostatic repulsion is induced between the surface charges while Coulomb's force is applied by the external magnetic field (36).

Action of these two electrostatic forces results in distortion of liquid drop into a conical shape called the Taylor's cone. Once the force of the electrostatic interactions overcomes the surface tension of the polymer solution, the liquid is ejected from the spinneret as a jet stream that then undergoes stretching and whipping to form a single continuous fiber (37). Solvent present in the polymer solution evaporates, effectively reducing the diameter of the fiber to a few nanometers. Finally, the charged fiber is deposited by attraction to a grounded collector. Depending upon the balance of the forces acting upon the polymer solution in the spinneret, droplets may also be formed instead of a single long continuous fiber (38).

8.3 Control of Nanofiber Morphology

The necessary pre-requisites for electrospun nanofibers are such that the nanofibers need to be of the same specified diameter throughout their length, be free of surface defects and be collected as single, continuous fibers (36).

Diameter of nanofibers is the most important factor influencing the quality of the electrospun mat. The two major factors affecting nanofiber diameter are jet size and the polymer concentration (36). Jet size may affect the fiber diameter such that the polymer stream while travelling from the jet to the collector may split into two or more streams, resulting in multiple fibers of varying diameter instead of one fiber of consistent diameter (Figure 3) (39).

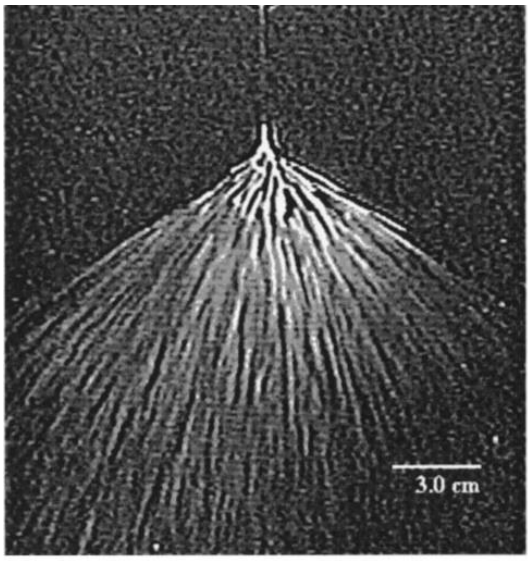

Figure 3: Single nanofiber jet splitting into multiple streams. Adapted from ((39))

Besides splitting, the nanofiber diameter is also affected by viscosity of the polymer solution; higher the viscosity, larger the fiber diameter. Polymer concentration is related to fiber diameter by a power law relationship. Fiber diameter is thought to be proportional to the cube of the polymer concentration (40).

Fiber diameter is also influenced by the electrical voltage applied during electrospinning. Larger voltage results in ejection of more fluid from the jet, hence fiber diameter will be greater (40). Consequently, the flow rate and applied voltage are also related by power law dependence between the two (30)(40).

Another issue with electrospinning is the formation of beads and pores in the nanofibers. Bead formation is influenced by polymer concentrations. Generally, higher concentration results in formation of fewer beads than polymer of low concentration (30)(40).

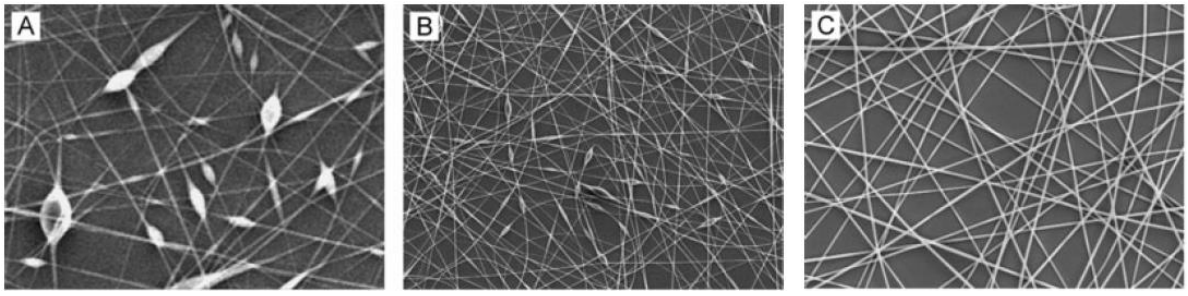

Figure 4: Electrospun nanofibers of poly (vinyl pyrrolidone) (PVP) at weight percent (A) 3%, (B) 5% and (C) 7%. Adapted from (36).

9. Aims and Objectives

The aim of this study was to develop 3-D bone scaffolds which will function as ECM, have sufficient mechanical strength for support in bone repair under load conditions and have a viable attachment mechanism for use in long bone fractures.

Electrospun membranes are limited in thickness and strength and so need to be compensated for these limitations. This study proposed the addition of mold casted polymeric sheets to the electrospun scaffold in order to augment for these limitations. Additionally, current fixation mechanisms for scaffolds involve either suturing, which may cause further trauma to the site of injury, or use of fibrin glue, which provides weak fixation. In this study, an alternate to these techniques is proposed by use of seamless polymeric tubes that are elastic in nature and so can be wrapped around the scaffold and provide a fixed point of attachment to the fractured bone.

The objectives of this study were to:

1. Develop a CAD model for device representation
2. Optimize parameters for electrospinning of PVA
3. Fabricate polymeric electrospun mats that will act as ECM for cell support
4. Fabricate mold casted polymeric sheets for improving mechanical properties
5. Build up a stacked layer in order to achieve 3-D scaffold
6. Fabricate polymeric sleeve for scaffold fixation
7. Characterize the features of the device using various testing modules

CHAPTER TWO

Literature Review

1. Poly (vinyl alcohol)

Poly (vinyl alcohol) (PVA) is formed by either full or partial hydroxylation of poly (vinyl acetate) (PVAc) (41). The degree of hydrolysis can be increased or decreased and is important for determining the various properties of the polymer (42). PVA is highly soluble in water but insoluble in organic solvents. High degree of hydrolysis results in lower solubility of PVA in water, therefore it typically dissolves at temperatures above 70ºC.

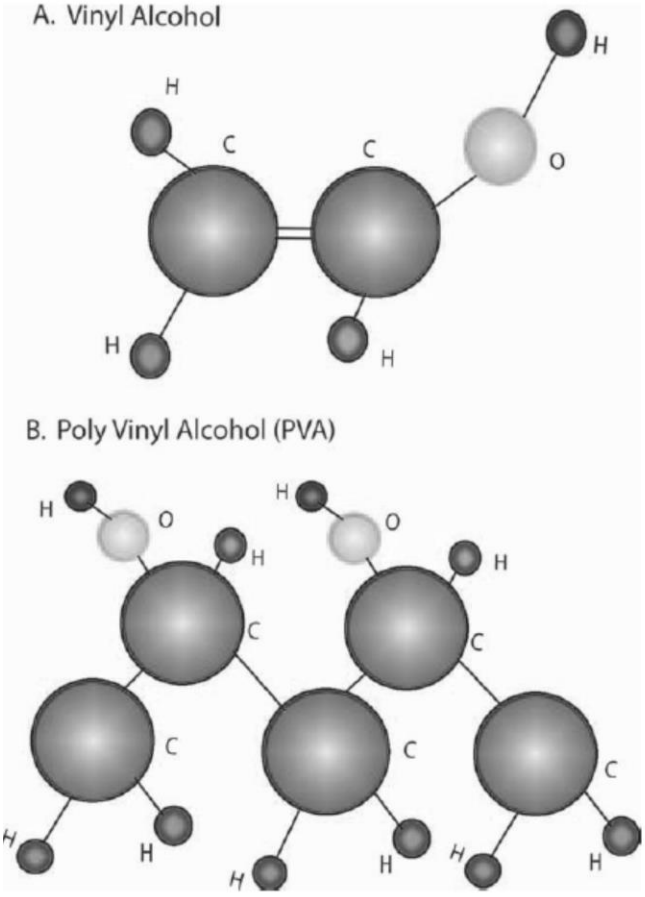

Figure 5: Structure and chemical composition of (A) vinyl alcohol and (B) PVA (Adapted from (41))

Degree of PVA hydrolysis can be from 80% to 99%; hydrogels are commonly obtained using PVA that has undergone almost complete hydrolysis. Hydrogel formation is initiated by cross-linking between linear polymers to form the gel phase (PVA) within the fluid (water) content. Low amount of polymer leads to soft hydrogel formation due to presence of greater fluid content whereas higher polymer concentration leads to stiffness within the material (41).

PVA has a proven history of biocompatibility owing to its use in a range of implantable medical devices. Medical uses of PVA include use of particulate PVA for treatment of vascular embolism (43), fabrication of hydrophilic coatings to encourage neurologic regeneration (44) and use as tissue adhesion barriers (45). The solubility of PVA in water and its non-toxic by-products enable its safe use for tissue engineering applications.

1.1 PVA in Cartilage Repair

PVA hydrogels, owing to their ability to sustain high water content and reasonable elastic and compressive properties can be used in cartilage repair (41). PVA hydrogels having concentration of 30% and higher have water content similar to healthy cartilage (41)(46). Articular cartilage has tensile strength of 17 MPa (47) and compressive strength between 0.53 MPa and 1.82 MPa (48). PVA hydrogels having tensile strength in the range of 1-17 MPa (49) and compressive modulus in the range 0.0012 to 0.85 MPa can be fabricated; strength is dependent on polymer concentration and number of test cycles (50).

1.2 PVA in Bone Tissue Repair

Electrospun PVA scaffolds for use in bone tissue repair are aimed at mimicking the hierarchical structure of bone tissue. Composites of poly (vinyl alcohol) with natural fibers and ceramics such as cellulose (51) and hydroxyapatite (52) aim to mimic the architecture and mineral content of natural bone. Gao *et al.*, used a sol-gel process to deposit bioactive glass particles onto electrospun PVA nanofiber mats. They aimed to enhance the mechanical properties as well as bioactivity of the scaffold since bioactive glass has both these properties (23). The bioglass-coated mats showed better cellular integration compared to electrospun mats without the bioglass coating.

The use of composite blends in electrospinning allows for incorporation of materials within the electrospun mat that cannot be otherwise processed into nanofibers by this technique. Chahal *et al.,* used electrospinning to fabricate PVA/collagen composite based scaffolds, since pure collagen cannot be electrospun (51).

2. Membrane Stacking

Critical size defect (CSD) is defined as the minimum defect size across which bone tissue regeneration is not possible without external intervention (53). Critical defect models can be of calvarial or long bone, with rat and rabbit calvarial defect models having CSD of 8 mm and 15 mm respectively (54).

Scaffolds fabricated using electrospinning yield mats that are of a two-dimensional nature due to lack of thickness. Membrane thickness can be increased but the process takes several hours. Also, thickness of the membrane is limited due to charge build-up on the collector plate which repels incoming fibers and hence a 3-D scaffold mat is not easily obtained. A simple solution to resolving this issue is either by stacking scaffold layers and fusing them together or by introducing macrofibers within the electrospun mats such as by rapid prototyping.

Stacking can be achieved by several methods reported in literature and have various advantages and disadvantages associated with their use. Stacking can be achieved by binding several electrospun layers using hydrogel as the binding agent (55). Yang *et al.,* fabricated membranes using this method that yielded stacked samples of >200 µm (55). The study showed that cells seeded onto the electrospun nanofibers showed acceptable proliferation within the structure. Due to the use of hydrogel and thin electrospun mats, these 3-D structures are fragile in nature.

The use of thermally induced phase separation (TIPS) to fuse the electrospun layers together is advantageous since the method allows for additional pore formation within the structure (56). Vaquette *et al.,* used this process to fabricate scaffolds that achieved thickness of upto 5 mm (56). Mechanical characterization of the structure showed that the structure had compressive strength in the range of 0.14 MPa. Morphological analysis showed that some pores within the electrospun mats were blocked by the TIPS polymer, hence compromising overall porosity of the structure.

Another method of building up electrospun layers is by heat treatment using pressurized gas that can bind the layers together (57). Leung *et al.,* used heat sintering to improve the mechanical properties of the stacked structure which yielded compressive strength of upto 1.7 MPa (57).

Cold welding under high pressure is another technique used for fusing electrospun layers together (58). Madurantakam *et al.,* fabricated 3-D scaffolds using electrospun membranes that were stacked and compressed using a hydraulic press (58). Compression strength in the range 60 MPa were recorded for samples with mineral content. However, porosity of the structure was shown to be reduced as a result of the welding process.

3. Hybrid Scaffolds

Scaffold fabrication techniques such as rapid prototyping enable high reproducibility since polymer deposition is dependent on pre-defined computer aided design models (59). However, scaffolds fabricated using rapid prototyping methods have large pore and fiber size and so are not effective for cell attachment and proliferation (60). Park *et al.,* fabricated hybrid scaffolds using a combination of electrospinning and rapid prototyping that enabled simultaneous incorporation of electrospun fibers within the large scale scaffold fabricated by rapid prototyping (60).

4. Scaffold Attachment

Scaffold fixation for functional implants most commonly involves suturing, fixation using the scaffold material itself or use of a sealing agent such as fibrin glue (61). The pre-requisite is to provide a stable point of fixation to the implanted scaffold with minimal consequence to both the device and the area of application. Suturing can be via direct fixation of the scaffold to the site of tissue damage. Fixation by suturing can also be achieved by placing the scaffold within the defect and covering it with a naturally-derived membrane such as the periosteum and then suturing it in place (62). In the case of periosteum, issues associated with fixation include the detachment of the membrane from the region of defect as well as mechanical failure of the scaffold which can result from improper fixation methods.

CHAPTER THREE

Methodology

The following methodology pertains to design and fabrication of scaffolds using the processes of electrospinning and mold casting for use in load-bearing bone tissue applications. An attachment mechanism was fabricated in order to provide stable fixation to the device in vivo.

1. Methodology Design

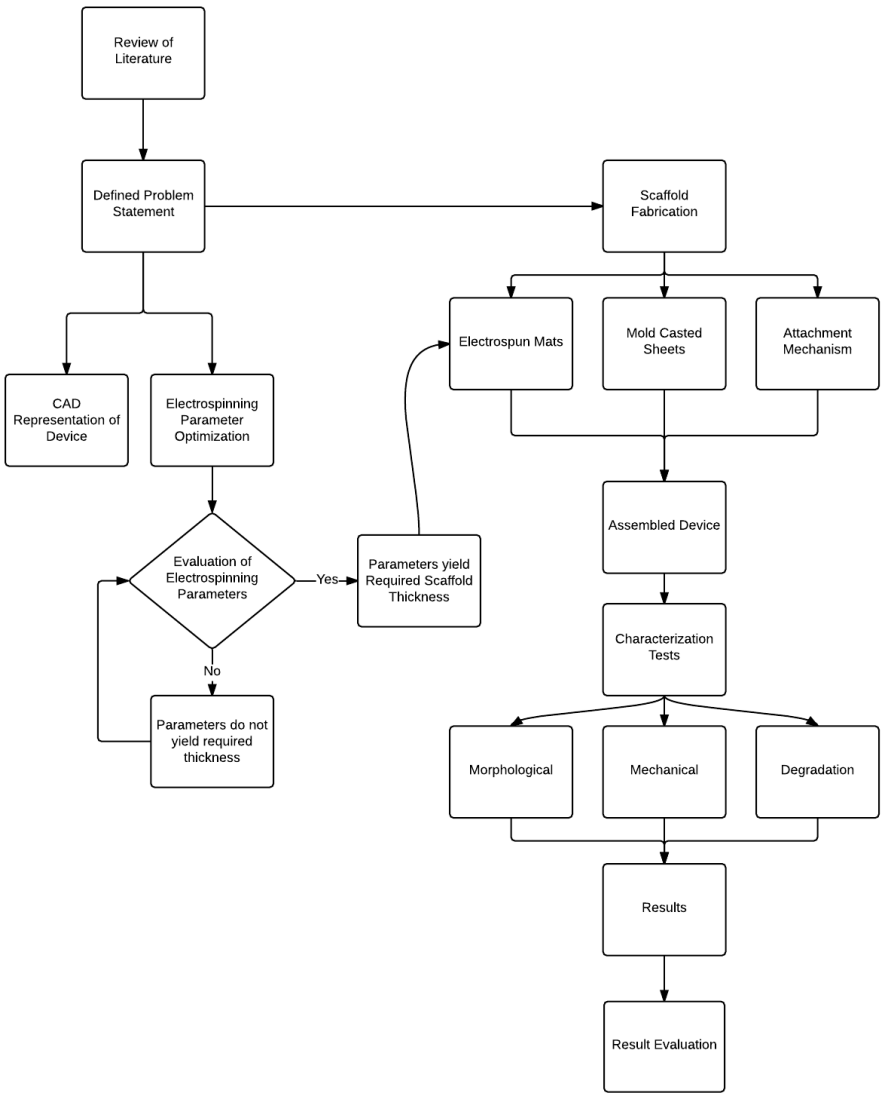

2. Experimental Protocol

The experimental protocol was initiated by generation of a CAD (computer-aided design) model depicting the scaffold design. Fabrication of the polymeric scaffold was done by using two techniques. Electrospun polymeric nanofiber based scaffolds were fabricated using electrospinning while macro sheets having dimensions on the scale of millimeters were fabricated using mold casting technique. The sheets were alternatively stacked in a layer-by-layer manner to obtain the thickness and strength needed for the structure. Attachment mechanism was subsequently fabricated for the obtained structure.

2.1 CAD Model of the Device

A CAD model of the device was generated using Pro/ENGINEER (Pro/E) (version PTC Pro/ENGINEER Wildfire 5.0) software. The design was generated as two part files (.prt format) that were later assembled (.asm format) to form the final scaffold structure.

The first part file was used to design the internal scaffold structure. The part was generated as extruded fibers, patterned at specific intervals in a repetitive manner along the x and y axis. Each pattern was generated such that, along the y axis, the fibers in the first pattern were at an angle of 45 degrees with the fibers in the second pattern and so on. For each pattern, 15 fibers of length 1500 were created along the x axis and the pattern replicated 6 times along the y axis at repeated intervals of fixed distance. In total, 5 patterns were generated in this manner, all having fibers in the x axis at 45 degrees to each other. A final file of the patterned fiber layers was generated such that the scaffold structure was in a circular form (Figure 6).

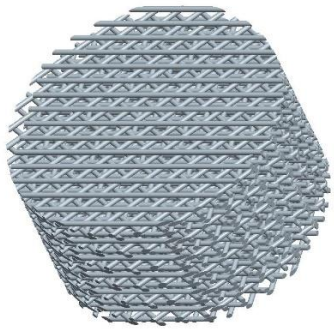

Figure 6: Scaffold Design

The second part file was created in order to design the attachment mechanism. A tubular structure was generated with dimensions on par with the scaffold design in the first part file. The two files were then assembled to obtain the device in its final form as shown (Figure 7).

Figure 7(a) and (b): Assembled Device

The device was demonstrated for bone defects using pre-modelled femur part file (Figure 8).

Figure 8: Bone Scaffold Demonstrated for Femur

2.2 Parameter Optimization

Optimization of electrospinning parameters was conducted in order to determine the working parameters for membrane formation using the polymer aqueous poly (vinyl alcohol) (aq. PVA).

2.2.1 Polymer Sample Preparation

Aqueous solutions of the polymer PVA of varying concentrations were prepared. PVA was purchased from BioChemica and was in the form of a fine, white powder (72000 BioChemica). The following percentage weight by volume formula was used to determine the amount of PVA and volume of distilled water used for preparing the solutions of different concentrations:

$$Weight\ Percent\ (w/v) = \left[\frac{Mass\ of of\ Solute\ (g)}{Volume\ of\ Solvent\ (ml)}\right] \times 100$$

Where the PVA concentrated as determined by weight percent (w/v) is represented by %.

The samples of aq. PVA were prepared by first determining the amount of PVA to be used for each concentration value. For instance, for 8% PVA, the amount of PVA in grams was calculated, using the formula given above, to be 3.2 g for 40 ml of water.

The calculated amount of PVA was measured using a weighing balance and added to the solvent in a glass beaker. The glass beaker was immersed in a water bath at room temperature and the temperature raised till 80ºC (PVA degrades rapidly at high temperatures). The required amount of PVA powder was gradually added to the beaker, accompanied by constant stirring until all the polymer had dissolved. The beaker was then removed from the water bath and the temperature of the solution brought back to room temperature. The aq. PVA solution was loaded into plastic syringes having 10 ml volume. The solution was then left overnight in order to remove bubbles in the solution which resulted from saponification of PVA during dissolution in the water bath.

2.2.2 Electrospinning Parameters

Electrospinning has a multitude of spinning parameters, all of which combined affect the scaffold fabrication process. In order to identify which parameters ensure adequate scaffold mat formation, a set of processing parameters was determined and the results subsequently evaluated.

The following three parameters were defined as parameters of interest for electrospinning in this experimental protocol:

1. Concentration of polymer solution
2. Voltage applied to the spinneret tip
3. Distance of collector plate from the tip of spinneret

Parameters were selected based on pre-determined experimental constraints normally reported to be encountered during the electrospinning process. For instance, low polymer concentration will lead to discontinuous spinning and bead formation (63). High polymer concentration leads to fibers that are not in the nanoscale (64). Additionally, at high

concentration, the spinneret tip becomes blocked due to polymer solidification at the tip and the process needs to be halted to remove the blockage and then commence with further spinning.

For the ES 1000 electrospinning unit, the following parameters had pre-determined limits. For voltage, the minimum voltage that could be applied for the current electrospinning setup was 5 kV while maximum voltage was 35 kV. Minimum distance from the spinneret tip to the collector plate at which electrospinning could be safely carried out was 80 mm. Maximum distance at which electrospinning can be conducted was 250 mm collector plate distance from the spinneret.

Based on these pre-requisites, the range of applied parameters to be optimized was determined. Three weight percent concentration values of aq. PVA were used for electrospinning, namely 8%, 12% and 16%. Voltage values used were of the range 10kV, 20kV and 30kV. Finally, the values used for distance of spinneret from collector plate were 120mm, 160mm and 200mm.

Electrospinning was performed using the Lab-scale Electrospinning Unit Electoris (ES 1000, Fanavaran Nano-Meghyas). The electrospun mats for parameter optimization and for all subsequent electrospinning experiments were collected on a flat, steel collector plate and later removed for further evaluation. All parameters for optimization were analyzed such that for one varying parameter, two electrospinning parameters were kept constant. Table 1 lists the parameters used for the optimization protocol.

Table 1: Parameters used for Electrospinning Optimization

PVA Concentration (%)	8	12	16
Voltage Applied (kV)	10	20	30
Distance from Spinneret (mm)	120	160	200

During the optimization process, the flow rate and maximum volume of solution injected were kept constant at 1 ml/h and 1 ml respectively. A 10 ml standard plastic syringe was used for electrospinning. The syringe, containing the polymer solution was loaded onto the syringe pump and the electrospinning pusher block was moved until the block was in contact with the syringe pump. Inner diameter of the 10 ml plastic syringe was determined to be 15.90 mm as given in

appendix A of the ES 1000 user manual. A stainless steel blunt end needle of 0.7 mm outer and 0.4 mm inner diameter was used for electrospinning.

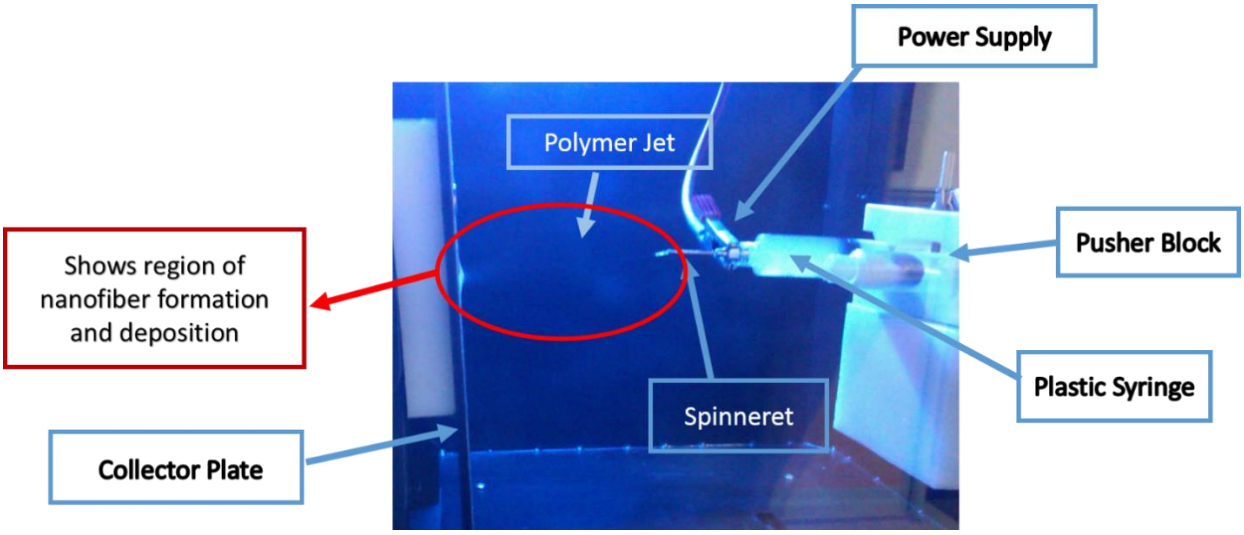

Figure 9: ES 1000 Electrospinning Unit

2.2.3 Optimization Results

The results of the electrospinning parameter optimization were analyzed qualitatively. The results were based on the thickness of the mat deposited on the collector, the absence of disruptions in the scaffold mat, the zone of deposition of polymer on the collector and the amount of polymer that was electrospun onto the collector plate. Disruptions in the electrospun mat occurred due to incomplete spinning of the polymer solution which led to the polymer accumulating as droplets on the surface of the collector.

Results were determined as good, average or bad. Good results showed well-formed scaffold mats with quantifiable thickness (quantifiable thickness was limited to 100 µm) and a small zone of deposition (Figure 10).

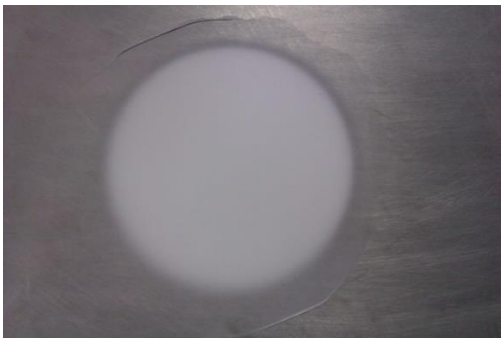

Figure 10: Scaffold mat showing good result as determined by the optimization protocol

Average results showed relatively well-formed membranes but were lacking in thickness and had a wider zone of deposition (Figure 11).

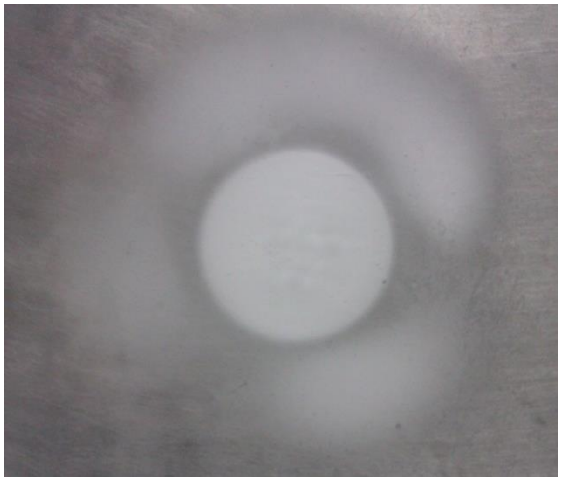

Figure 11: Scaffold mat showing average result as determined by the optimization protocol

Bad results showed poor-formed membranes with numerous disruptions in the electrospun mat due to partial spinning of the polymer sample and an extremely wide zone of deposition (Figure 12).

Figure 12: Scaffold mat showing bad result as determined by the optimization protocol

For the aforementioned electrospinning parameters, two sets of parameters were determined to yield good results. The first set of parameters to yield good results were 8% polymer concentration, 20kV applied voltage and 120 mm collector distance from the spinneret. Thickness of 600 µm was quantified. For the parameters of 16% polymer concentration, 30kV applied voltage and 120 mm collector distance, 300 µm thickness was determined. From these results, it was determined that the parameters of 8% polymer concentration, 20kV applied

voltage and 120 mm distance were optimum for the experimental conditions and were used for all subsequent electrospinning experiments.

Table 2: Results for 8% PVA concentration

Distance / Applied Voltage	120 mm	160 mm	200 mm
10 kV	Average	Bad	Bad
20 kV	Good	Bad	Bad
30 kV	Bad	Bad	Average

Table 3: Results for 12% PVA concentration

Distance / Applied Voltage	120 mm	160 mm	200 mm
10 kV	Bad	Bad	Average
20 kV	Average	Average	Bad
30 kV	Bad	Average	Average

Table 4: Results for 16% PVA concentration

Distance / Applied Voltage	120 mm	160 mm	200 mm
10 kV	Bad	Average	Bad
20 kV	Bad	Average	Bad
30 kV	Good	Average	Average

2.3 Scaffold Fabrication

The scaffold was fabricated using two techniques; electrospinning and mold casting. Due to the inherent limitation of achieving limited thickness in electrospun mats, mold casted layers were introduced within the structure. The device was stacked with the electrospun and mold casted arranged in an alternating manner until the required thickness was achieved. The following sections detail the process of scaffold fabrication and membrane stacking.

2.3.1 Electrospinning

Poly (vinyl alcohol) (PVA) solution of 8% concentration was electrospun at 20kV applied voltage with the distance from the tip of spinneret to the collector plate being 120mm. These parameters were determined as optimum for the electrospinning of poly (vinyl alcohol). The polymer was electrospun onto a grounded steel collector plate. The flow rate and volume of polymer injected were kept constant at 1ml/h and 1ml respectively for each electropun sample.

After the electrospinning process, the samples were carefully removed from the collector plate and subsequently sectioned into 20 mm by 20 mm square pieces using a sharp cutter blade and used for further processing (Figure 13).

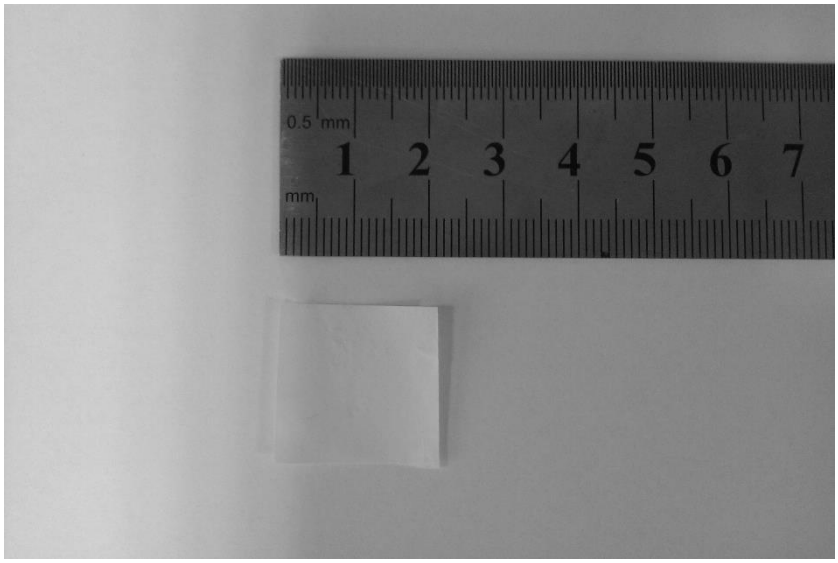

Figure 13: Electrospun PVA Mat

2.3.2 Mold Casting

Mold casted specimen of the polymer were introduced in order to build up scaffold thickness. The mold was fabricated on square steel blocks of 42 mm by 42 mm dimension using Computer Numerical Control (CNC) milling machine (MV-1060 YDPM) with a solid carbide end-mill of 1 mm diameter. The engravings were of 1 mm width at an interval of 1 mm and having depth of 0.5 mm. After the grooves were etched onto the surface, the steel block was positioned such that the previously engraved grooves were now at a 90^{o} angle. The engraving pattern was repeated as previously such that the final mold obtained contained interconnected grooves at regular intervals (Figure 14).

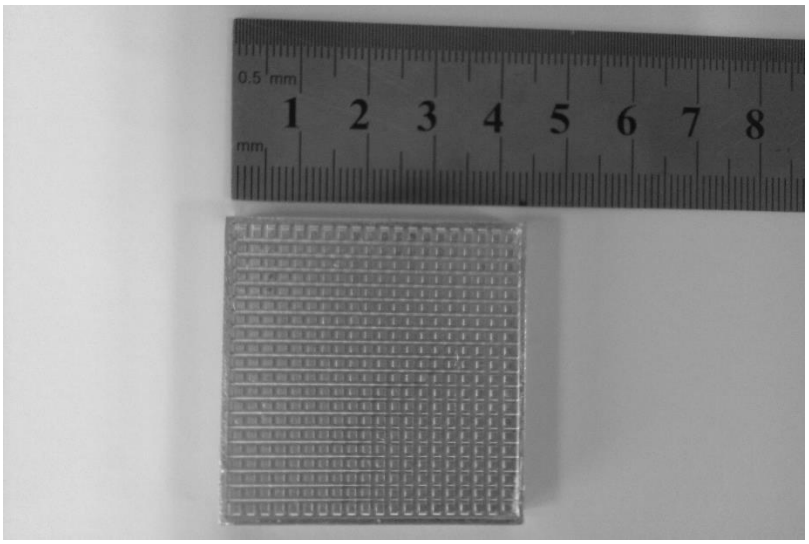

Figure 14: Mold for Casting

Polymer solution of aq. PVA having 20% concentration was prepared. High concentration enabled high viscosity to be achieved for PVA. The polymer was then casted by pouring the solution into the engraved pattern of the CNC mold. Excess polymer was scraped off and the mold was incubated at room temperature for 6 hours in order for the polymer to cure. After curing, the PVA sheet was removed from the mold. The PVA sheets obtained had dimensions of 4 mm by 4 mm and were further sectioned into 2 mm by 2 mm pieces as for the electrospun specimen.

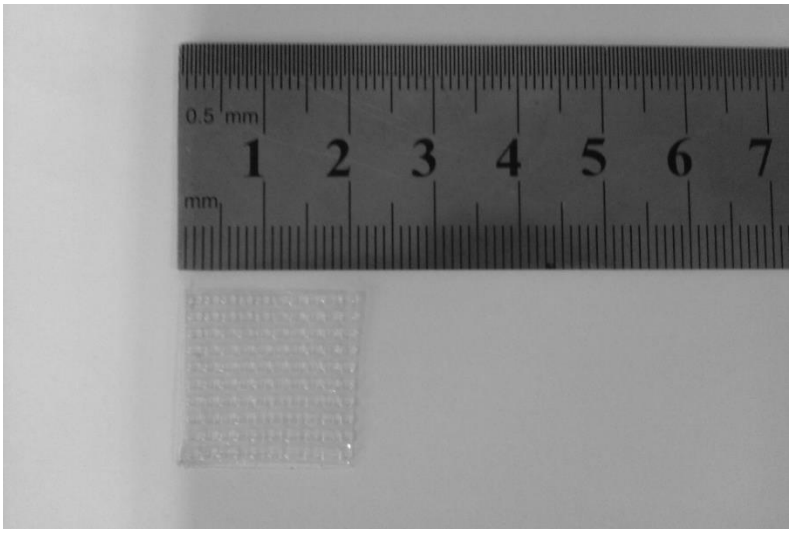

Figure 15: Casted PVA Sheet

2.3.3 Layer Stacking

Requirements for bone tissue scaffold include porosity and sufficient mechanical strength. Electrospun mats provide porosity and increased surface area essential to supporting tissue regeneration across the bone defect. However, scaffolds obtained solely via electrospinning are not mechanically strong. Casted sheets have greater mechanical strength but poor porosity. Therefore, stacking was used in order to incorporate the properties of both electrospun and casted specimen.

Stacking was done by bonding an electrospun mat to the casted sheet using PVA of 8% concentration as glue. The sheets were placed between a mechanical clamp and held in place for some time in order to ensure proper binding between the specimen. Electrospun and casted sheets were added intermittently to the structure until a final device of approximately 6 mm thickness was achieved.

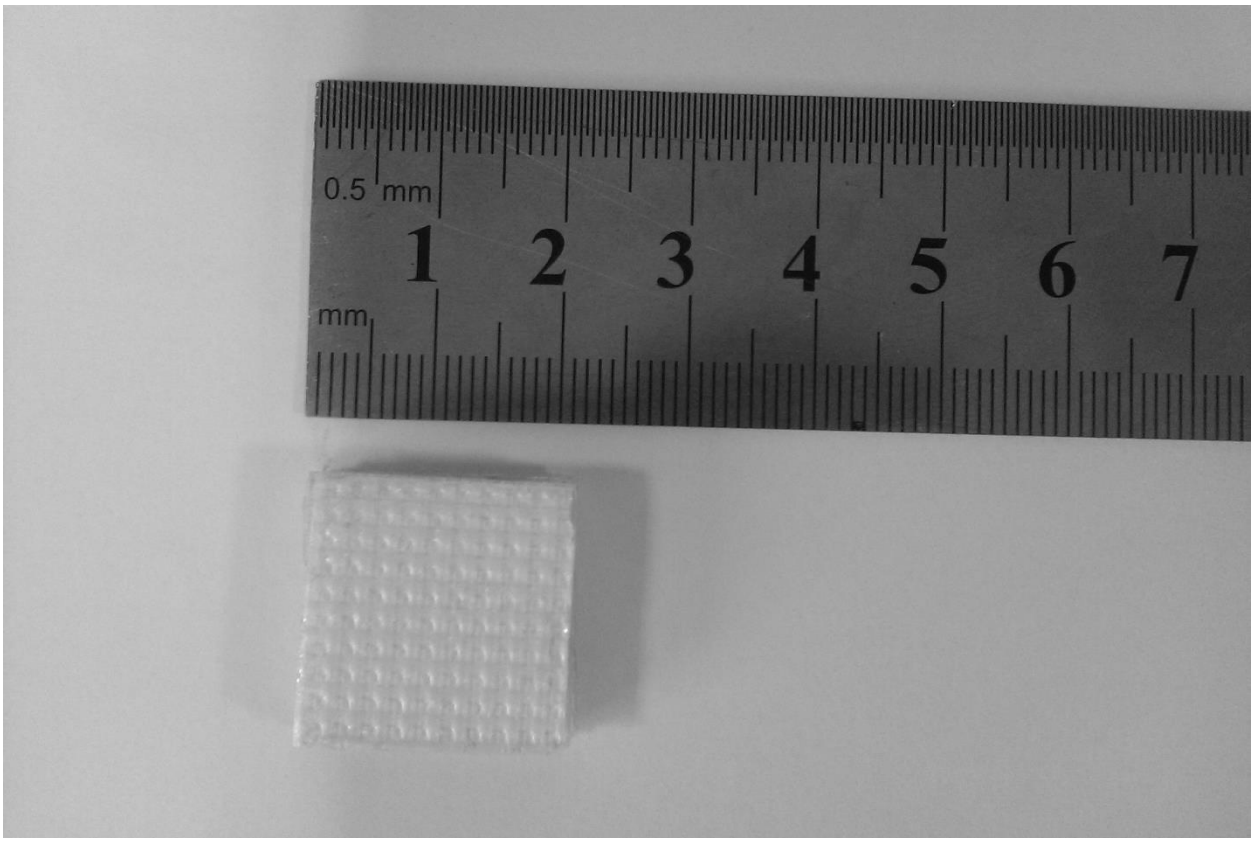

Figure 16: Stacked Scaffold

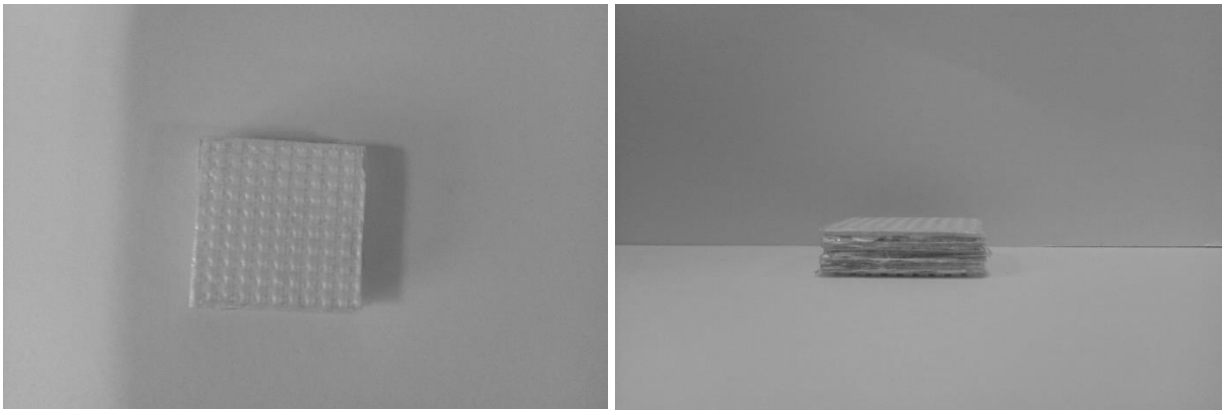

Figure 17 (a) and (b): The three-dimensional stacked scaffold

2.4 Fabrication of Attachment Mechanism

The attachment mechanism was fabricated using polyurethane (PUR) (PMC 744 Part A and B, SMOOTH-ON, Inc). This polymer is elastic and hence is easily stretchable so that it can conform to the desired shape. The attachment sleeve was fabricated by first mixing PUR part A and B in a 2:1 ratio. In total 6 ml of PUR was made by mixing 4 ml part A and 2 ml part B. The mixture was poured into a mold shaped into a hollow tubular crevice. The crevice was created by placing a solid plastic tube of 16.3 mm outer diameter within a hollow plastic tube of 19.3 mm inner diameter. The mixture was poured with this mold and incubated for 12 hours to allow for curing. The casted sleeve was subsequently removed from the plastic mold. The sleeve fabricated had a diameter of 3 mm and length 40 mm. The stacked scaffold fabricated previously was cut into circular discs having a diameter of 20 mm and inserted into the attachment sleeve to obtain the final device.

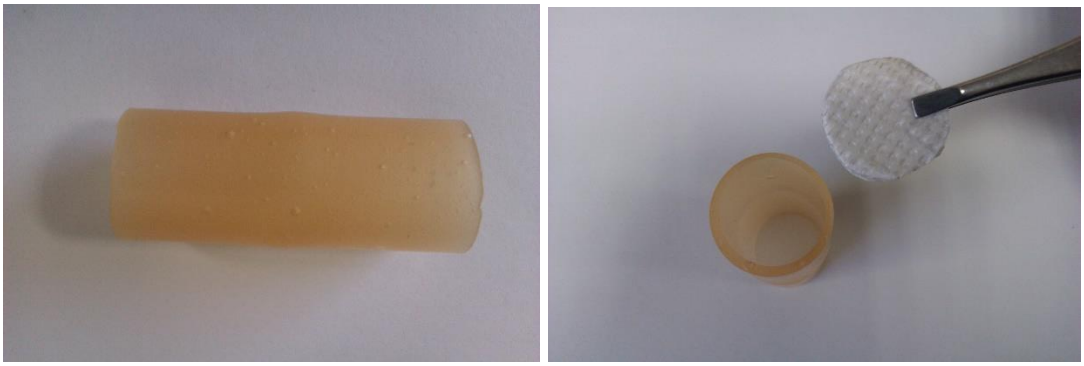

Figure 18: The figure shows (a) the casted polyurethane sleeve and (b) assembly of stacked scaffold and attachment sleeve

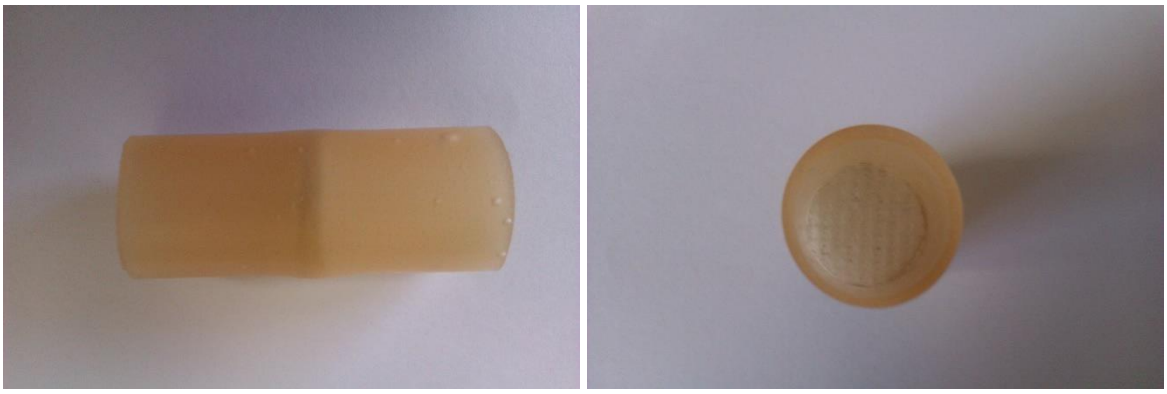

Figure 19: Assembled device; (a) Side view and (b) Top view

2.5 Scaffold Characterization

The scaffold samples were analyzed for their morphological, mechanical and degradation properties.

2.5.1 Morphological Characterization

For morphological analysis, scanning electron microscope (SEM) (MIRA3 TESCAN Field Emission Scanning Electron Microscope) was used. Four specimens were analyzed including casted PVA sheet, electrospun mat collected on collector plate, electrospun mat collected on rotating mandrel and stacked scaffold. All samples were first coated with gold particles using ion coater (QUORUM Q150T ES) and imaged at 5kV.

2.5.2 Mechanical Characterization

Mechanical characterization was done using universal testing machine (UTM, SHIMADZU AG XPlus 20kN). Two stacked scaffold samples of dimensions 20 x 20 x 6 mm (average) were tested for compressive strength. The compressive load was applied at cross-head speed of 0.5 mm/min. Average initial displacement for the samples was 6 mm and the load was applied until displacement was seen to be 0 mm on the UTM output screen. Stress/strain values were obtained from this method and a graph was plotted. Young's modulus of compression which lies within the linear region of the stress/strain graph was calculated as:

$$E = \frac{\sigma}{\epsilon}$$

Where E = Young's Modulus of compression, σ = stress at yield point and ϵ = strain at yield point.

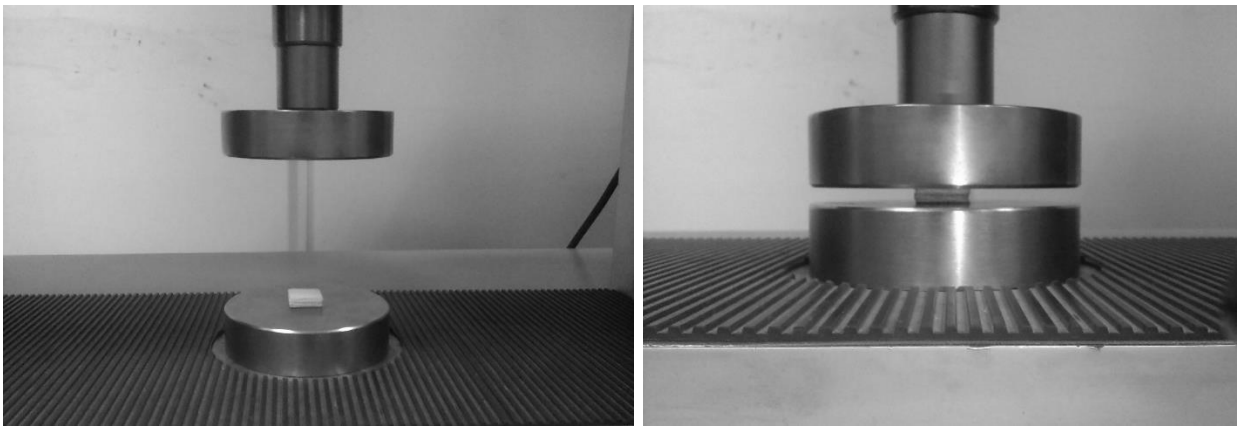

Figure 20: Mechanical testing of stacked sample

2.5.3 Degradation Properties

Degradation rate of the samples was determined in vitro using phosphate buffer saline (PBS, pH 7.4 - bioWORLD). The solution was prepared by dissolving 4 tablets of PBS in 100ml water. The samples were weighed before being completely immersed in 20 ml of PBS in a beaker and incubated at 37ºC (Figure 21). The samples were removed and the PBS solution drained at intervals of 30 minutes. The samples were dried and measured for loss in weight over time. The PBS solution was refreshed for each time interval and the samples re-immersed.

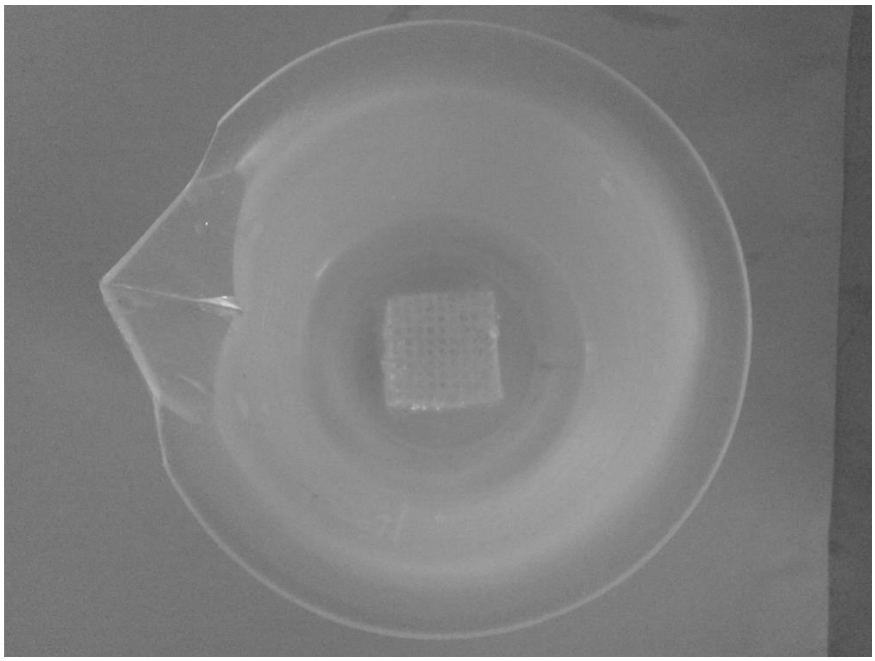

Figure 21: Scaffold immersed in 20 ml of PBS solution

2.6 Chemical Testing

Fourier transform infrared spectroscopy (FTIR) was used in order to compare chemical bonding between PVA and hydroxyapatite (HA) blend. Hydroxyapatite mimics the chemical composition of bone mineral and hence enables functionalization of the scaffold. PVA and HA blends were prepared using a 2:1 ratio for PVA and HA respectively. 2% HA solution was prepared by dissolving 0.4 g HA in 20 ml distilled water. 8% PVA solution was prepared using 40 ml distilled water and 3.2 g PVA. The 2% HA solution was mixed with 8% PVA and the mixture stirred vigorously, using a glass rod, in order to obtain the PVA/HA blend. PVA and PVA/HA samples were then cast as thin films at room temperature. FTIR (PerkinElmer Spectrum 100 Series) was used to analyze the casted PVA and PVA/HA samples for comparison.

CHAPTER FOUR

Results

1. Scanning Electron Microscope

The images obtained using SEM imaging demonstrates the morphology of the scaffold device. The casted PVA sample was imaged and diameter of the open pore was measured to be 946.95 µm when viewed at a magnification of 157 X as shown below (Figure 22).

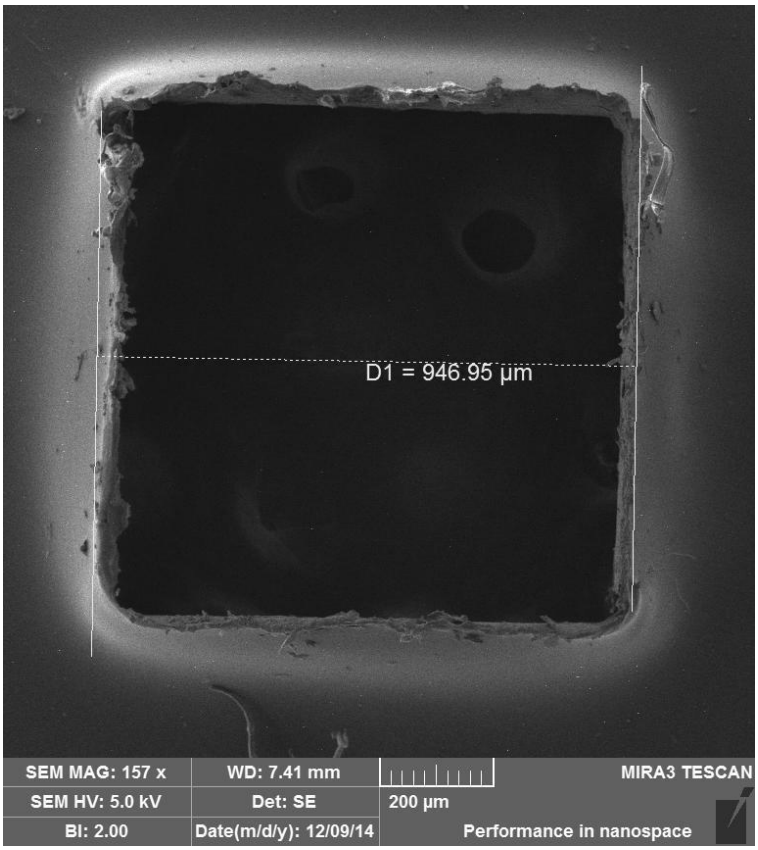

Figure 22: SEM image of casted PVA sheet

Electrospun mat collected on collector plate was imaged at a magnification of 50000 X in order to observe fiber morphology. Average fiber size of 87.42 ± 38.53 nm was observed while average pore size of 0.5 µm was seen (Figure 23 (a)). Electrospun mat collected on rotating mandrel was imaged at 25 000 X (Figure 23 (b)).

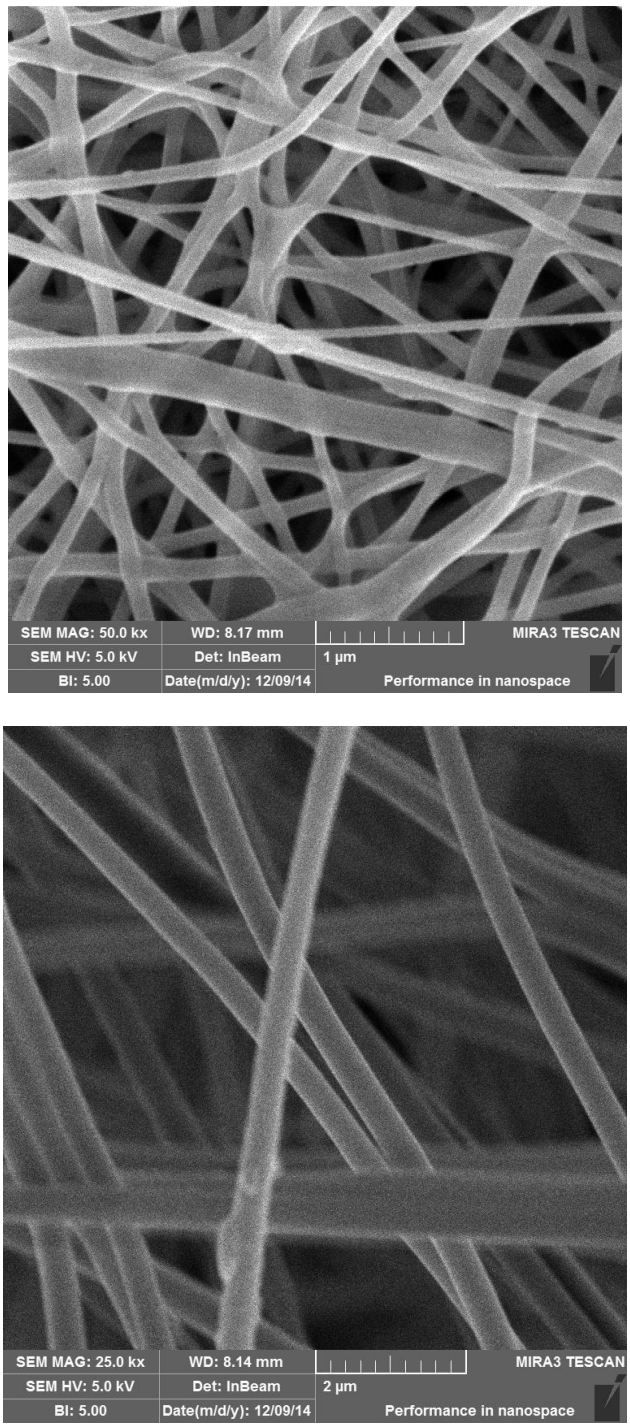

Figure 23: SEM image of (a) electrospun mat on collector plate and (b) electrospun mat on rotating mandrel

The image of the stacked scaffold at 51 X shows four units of casted PVA sheet while the image at 131 X magnification shows a single subunit with the electrospun mat visible through the open pore. The electrospun mat is further imaged at 5000 X magnification to view the electrospun mat (Figure 24 (a), (b) and (c)).

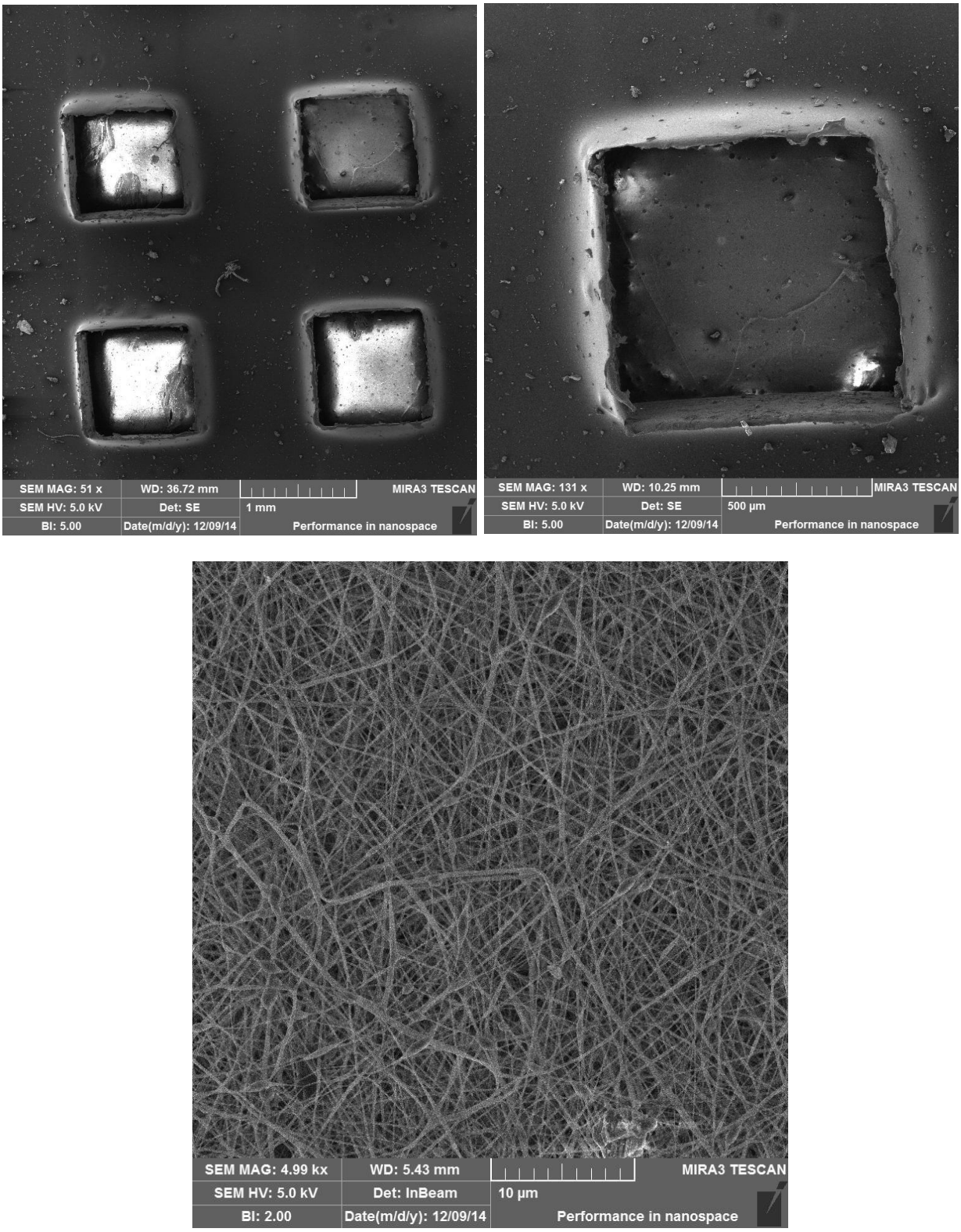

Figure 24: SEM image of stacked scaffold at (a) 51 X, (b) 131 X and (c) 4990 X

2. Universal Testing Machine

The two stacked samples had initial thickness of 5.8 mm and 6.2 mm (6 ± 0.14 mm) and final thickness after compression was 2.5 mm and 2.0 mm (2.25 ± 0.35 mm). After maximum compression, the compressed samples showed a relative degree of elasticity evidenced by an increase in thickness of the samples. Scaffold thickness six days after compression testing was observed to be 3.9 mm and 4.5 mm (4.2 ± 0.42 mm). Maximum stress was observed to be 50 N/mm^2 and 46 N/mm^2 (48 ± 2.82 N/mm^2) for maximum strain rate of 90% and 103% (96.5 ± 9.19%) respectively (Figure 25). Maximum force applied for maximum strain was 20000 N for both samples.

Using the stress/strain graph, the yield point was determined to be where the graph became non-linear and there was a greater increase of stress for less increase in the amount of strain. The yield points were 5 N/mm^2 and 3.1 N/mm^2 (4.05 ± 1.34 N/mm^2) at 65% and 75% (70 ± 7.07%) strain rate respectively. Hence, the Young's Modulus for compression (MPa) for both yield points was calculated as 0.07 MPa and 0.041 MPa (0.05 ± 0.02 MPa) respectively. The compressive strength (S, MPa) at maximum stress and strain was 0.55 MPa and 0.44 MPa (0.49 ± 0.07 MPa).

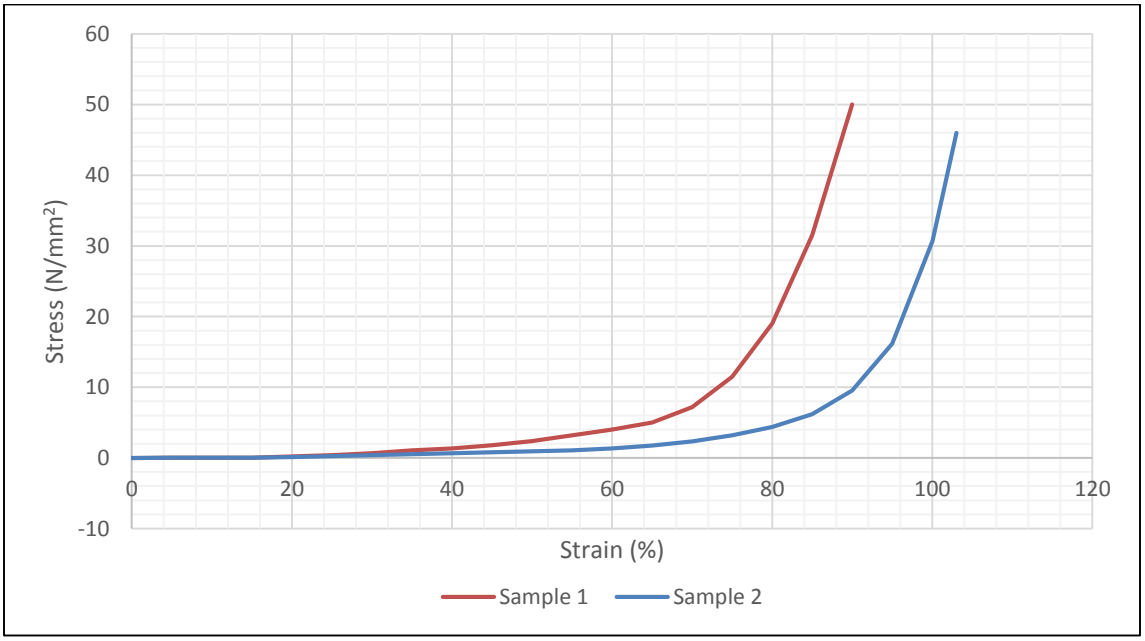

Figure 25: Stress/Strain Graph

3. In vitro Degradation Analysis

The initial mass of the sample after 30 mins of immersion was measured to be 1360 mg using a weighing balance. The sample took 270 mins to degrade completely. During the first 90 mins of the testing, there was a rapid decrease in weight of the sample. A significant increase in sample weight was observed at 150 mins, most likely due to increased hydration of the polymeric material. The sample then continued to show loss in weight over time. At 210 mins, the sample was separated into two large but still quantifiable chunks while after a further 30 mins, the sample had dispersed significantly and mass could not be quantified. The sample completely dissolved at 270 mins from the start of the experiment. Table 5 shows the degradation results obtained during this experiment.

Table 5: Sample degradation over time

Time (mins)	30	60	90	120	150	180	210	240	270
Sample Weight (mg)	1360	1266	1180	1190	1449	1442	1317	Mass not quantified	Sample dissolved

4. Fourier Transform Infrared Spectroscopy

The typical waveform for PVA showed –OH bond at v = 3200 – 3470 cm^{-1} while $–CH_2$ symmetric and asymmetric stretching was observed at v = 2938 cm^{-1}. The –CH stretching vibration was observed at the shoulder-like band at v = 2850 cm^{-1}. The PVA/HA spectrum showed decreased intensity due to decreased amount of PVA. Intensity was observed to increase at v = 1375 cm^{-1} due to presence of PO_4^{-3} group in the sample.

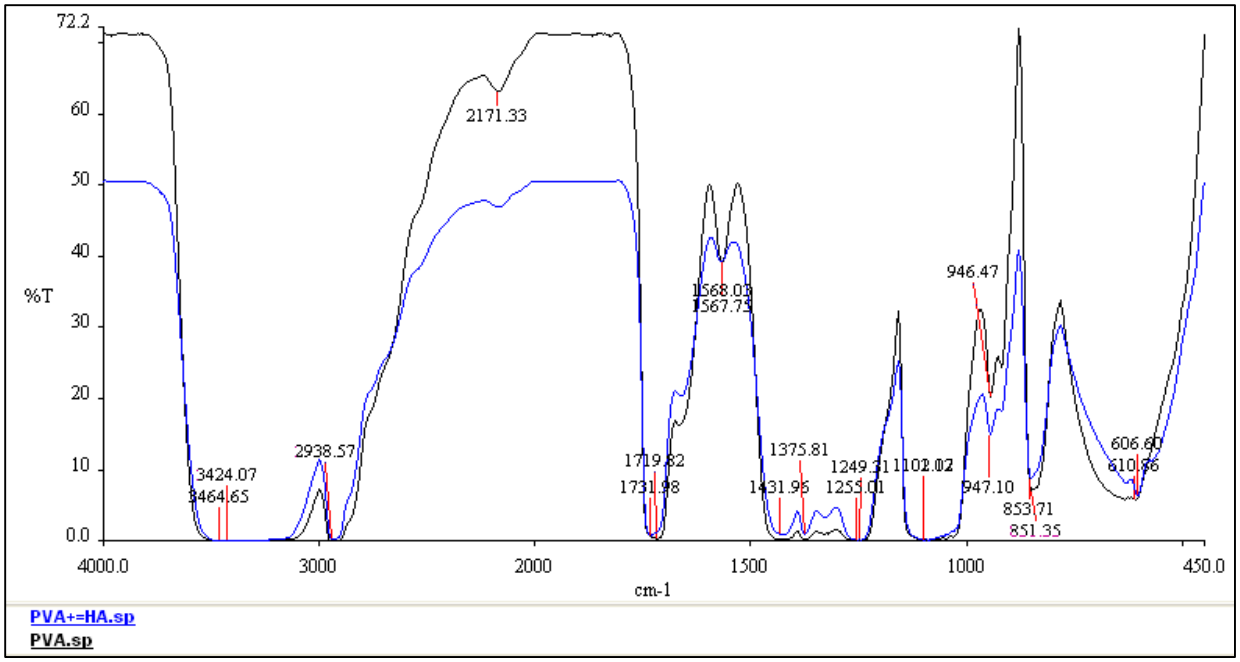

Figure 26: FTIR of PVA and PVA/HA casted sheets. The blue waveform represents HA/PVA casted specimen while the black waveform represents PVA casted specimen.

CHAPTER FIVE

Discussion

The objective of this study was to design and fabricate artificial scaffolds for segmental bone defects that contain microstructural properties, i.e. porosity and support, for effective cellular integration and macro structural properties, i.e. bulk and mechanical strength, to sustain load bearing forces when implanted in the body. The scaffold was aimed to be deployed using an attachment mechanism that could eliminate conventional scaffold fixation techniques and provide a stable point of attachment for use in long bone fractures.

A 3-D scaffold device that can be manufactured using the methodology used in this study can be advantageous to current efforts for development of suitable synthetic bone graft substitutes. Electrospinning is a versatile technique for scaffold fabrication but has limitation in thickness and mechanical integrity. Augmentation of electrospinning with another fabrication method that can provide structural support is hence desirable. Electrospinning can be augmented using techniques such as rapid prototyping as demonstrated by (60). However, such methods require custom-built apparatus which may not be a feasible option in most cases. Our study uses techniques that are relatively inexpensive to fabricate a porous, 3-D scaffold with reasonable mechanical properties.

In this study, a 3-D scaffold a device was constructed using a combination of electrospinning and mold casting in order to integrate the properties required for a functional bone scaffold. The scaffold was subjected to a series of characterization tests and the results subsequently analyzed.

The results for SEM analysis showed that for casted specimen, diameter of each square was 946.95 μm while for electrospun mats, nanofiber diameter was determined to be 87.42 ± 38.53 nm and pore size of 0.5 μm. For UTM analysis, results showed that Young's Modulus for compression (MPa) for yield point 0.05 ± 0.02 MPa while the compressive strength (S, MPa) at maximum stress and strain was 0.49 ± 0.07 MPa. Degradation analysis showed that the scaffold disintegrated 270 mins after dissolution in PBS.

1. SEM Analysis

Morphological observation of the device components showed nanofiber size of 87.42 ± 38.53 nm and pore size of 0.5 µm in case of electrospun scaffold fabricated on collector plate. Studies show that average pore size of ~100 µm is optimum for bone tissue since greater porosity can lead to mechanical failure of the scaffold (65). The present pore size of the electrospun layer was less on account of the fact that electrospinning time was extensive and each electrospun mat took an hour of deposition to achieve the required thickness for this study. Analysis of the stacked scaffold samples showed that the casted and electrospun layer integrated well and there was no visible disruption to the electrospun mat due to use of PVA glue as binding agent or from mechanical handling of the structure during the stacking process.

2. UTM Analysis

Compression testing showed that the samples had maximum compressive strength of 0.49 MPa. This strength was better than mechanical strength of the scaffold fabricated by Vaquette *et al.,* which had compressive strength of 0.14 MPa (56). The mechanical strength was weak compared to those of scaffolds fabricated by Leung *et al*., which had compressive strength in the range of 1.7 MPa (57). The scaffolds fabricated by Madurantakam *et al*., had the highest compressive strength of 60 MPa (58). However, their fabrication method of cold welding yielded scaffolds that had little porosity.

Stress shielding is an important phenomenon in bone tissue regeneration. Traditionally, metals and ceramics that have mechanical strength greater than that of bone are the preferred implant material for bone repair. However, these implants are prone to failure since the implant material bears most of the loading stress while bone tissue experiences little or no loading stress. Continuous loading can lead to mechanical wear of the implant; being brittle in nature, such implants consequently have greater susceptibility to mechanical failure. Additionally, since bone tissue experiences no loading stress, bone remodeling is affected. Bone tissue remodeling is dependent on mechanical loading and stress shielding by metal and ceramic implants hampers this process.

Polymeric implants for bone repair have low stress shielding effect since mechanical strength is lower than that of bone. It was observed during this experiment that the stress/strain

graph remained linear across a large change in strain for low increase in stress. This shows that upto the yield point (0.05 ± 0.02 MPa), there was more displacement for the given stress. After yield point, there was little change in displacement while stress increased rapidly until maximum stress at 48 ± 2.82 N/mm^2.

Both tested specimen were observed to revert to the original displacement after load was removed. The specimen initially showed 2.25 mm thickness after compression which increased to 4.2 mm after some time. This highlights the stress shielding effect of polymeric scaffolds that can be beneficial to bone remodeling in vivo.

3. Degradation Analysis

The scaffold sample degradation showed increase in scaffold mass at time 150 mins from sample immersion in PBS. This was due to the hydrophilic nature of the substance which lead to water retention within the structure when the PBS solution was removed. Degradation time maxed out at 270 mins since volume of the PBS solution was in excess of physiological conditions in order to fully immerse the sample. Reduced amount of PBS can be key to reducing degradation time as can treatment of the PVA scaffold using techniques such as irradiation to increase cross-links between PVA sheets. The sample did not disintegrate at first and retained its shape for the first 210 mins after which a smaller fragment of the sample broke off from the main. The scaffold sample dissolved completely after 270 mins of immersion. The degradation time for PVA scaffold can be improved by use of cross-linking methods such as glutaraldehyde or irradiation methods. However, such methods can result in a compromise of the biocompatibility of the scaffold.

4. Chemical Analysis

FTIR was performed using PVA and HA/PVA casted sheets. Scaffolds for bone tissue engineering require materials that mimic the mineral content of natural bone in order to induce osteointegration. This analysis was performed in order to observe HA/PVA interaction in the form of a single blend. The FTIR analysis of HA/PVA sample showed the characteristic phosphate peak at v = 1375 cm^{-1} that indicates the presence of HA within the structure.

5. Attachment Mechanism

The attachment mechanism was casted as a seamless tube using polyurethane. The polymer in question was chosen since it is elastic in nature. Hence, it can easily wrap around long bone ends in segmental defects and consequently enable easy insertion of the 3-D scaffold in vivo. It was deduced that reduction in elasticity can confer greater fixation ability to the structure. However, this is beyond the scope of the present study.

CHAPTER SIX

Conclusion

This research focused on a conceptual design for a bone scaffold prototype that can function as an ECM for bone growth, have sufficient mechanical strength and a deployable attachment mechanism. The study showed that a 3-D scaffold could be fabricated using two separate fabrication methods; electrospinning and mold casting.

The study was initiated by developing a 3-D Cad model for device representation and for analysis of the attachment mechanism using a pre-modelled femur design. It was determined that attachment sleeve fabricated from a flexible polymer can enable scaffold fixation in long bones.

During thus study, electrospinning parameters were optimized for poly (vinyl alcohol) and scaffold properties obtained according to the study requirements. It was determined that PVA mats fabricate using processing parameters of 8% PVA concentration, 20 kV applied voltage and 120 mm collector plate distance from the tip of spinneret. A 3-D scaffold of thickness 6 mm was then fabricated using electrospinning and mold casted specimen. A simple attachment mechanism was demonstrated for scaffold fixation in long bone segmental defects. This can lend greater stability to the structure when it is deployed in vivo.

Morphological analysis revealed that pore size for electrospun mats was 0.5 µm which is lower than the optimum pore size for bone tissue. Additionally, SEM imaging showed that there was no visible damage to the electrospun membrane during stacking. Mechanical strength was analyzed and compared to existing literature. It was found that the mechanical strength was greater than that of (56) and less than that of (57). Degradation testing showed that the 3-D scaffold dissolved in PBS solution after 270 mins of immersion. The attachment mechanism was fabricated using PUR which is elastic in nature. Hence, scaffold fixation using this method can provide better stability compared to existing methods of fixation.

Future Work

Osteointegration properties of the stacked structure can be improved by incorporating hydroxyapatite within the structure. This can subsequently affect the mechanical properties of the resulting device. Degradation rate can also be decreased by use of various techniques. In vitro cell culture testing of the device can reveal the efficiency of cellular integration and migration within the structure. In vivo testing using animal models can be used to account for both cellular integration and mechanical stability of the scaffold.

The 3-D scaffold can be fabricated using mineral content other than HA, such as ceramics. Composite scaffolds can be fabricated using other polymers such as PCL that can enable improvement of mechanical as well as degradation properties. Fabrication of biodegradable attachment sleeve can be advantageous to this device. The degradation rate for the attachment mechanism may be such that the sleeve degrades well after the rest of the scaffold has degraded in order to provide stability to the healing tissue. Optimization and mechanical characterization of the attachment sleeve can enable better evaluation of its viability in vivo.

REFERENCES

1. Joseph P. Vacanti, Robert Langer. Tissue Engineering. Science. 1993 May 14;260(5110):920–6.

2. Dietmar W. Hutmacher. Scaffolds in tissue engineering bone and cartilage. Biomaterials. 2000 Dec 15;21(24):2529–43.

3. Ami R. Amini, Cato T. Laurencin, Syam P. Nukavarapu. Bone tissue engineering: Recent advances and challenges. Crit Rev Biomed Eng. 2012;40(5):363–408.

4. Edward. M. Younger, Michael. W. Chapman. Morbidity at bone graft donor sites. J Orthop Trauma. 1989;3(3):192–5.

5. Christian Delloye, Olivier Cornu, Vincent Druez, O. Barbier. Bone allografts: What they can offer and what they cannot. J Bone Joint Surg Br. 2007 May 1;89-B(5):574–80.

6. A. Seth. Greenwald, Scott. D. Boden, Victor. M. Goldberg, Yusuf. Khan, Cato. T. Laurencin, Randy. N. Rosier. Bone-graft substitutes: Facts, fictions, and applications. Am Acad Orthop Surg 75th Annu Meet J Bone Jt Surg. 2001;83-A Suppl 2 Pt 2:98–103.

7. Usha Kini, B. N. Nandeesh. Physiology of Bone Formation, Remodeling, and Metabolism. In: Ignac Fogelman, Gopinath Gnanasegaran, Hans van der Wall, editors. Radionuclide and Hybrid Bone Imaging. Springer Berlin Heidelberg; 2012. p. 29–57.

8. Jeffrey O. Hollinger, Thomas A. Einhorn, Bruce Doll, Charles Sfeir, editors. Bone Tissue Engineering. 1 edition. Boca Raton: CRC Press; 2004. 352 p.

9. Bart Clarke. Normal Bone Anatomy and Physiology. Clin J Am Soc Nephrol. 2008 Nov 1;3(Supplement 3):S131–9.

10. Dobnig H, Turner RT. Evidence that intermittent treatment with parathyroid hormone increases bone formation in adult rats by activation of bone lining cells. Endocrinology. 1995 Aug;136(8):3632–8.

11. Boron WF, Boulpaep EL. Medical Physiology: A Cellular and Molecular Approach. 2nd Revised edition edition. Philadelphia, PA: Saunders; 2008. 1352 p.

12. Stevens MM. Biomaterials for bone tissue engineering. Mater Today. 2008 May;11(5):18–25.

13. Chao Le Meng Bao, Erin Y.L., Mark S.K., Yuchun Liu, Mahesh Choolani, Jerry K.Y. Advances in Bone Tissue Engineering. In: Jose A. Andrades, editor. Regenerative Medicine and Tissue Engineering. InTech; 2013.

14. William R. Moore, Stephen E. Graves, Gregory I. Bain. Synthetic bone graft substitutes. ANZ J Surg. 2001;71(6):354–61.

15. Hench LL, Polak JM. Third-generation biomedical materials. Science. 2002 Feb 8;295(5557):1014–7.

16. Chen Q, Zhu C, Thouas GA. Progress and challenges in biomaterials used for bone tissue engineering: bioactive glasses and elastomeric composites. Prog Biomater. 2012 Sep 26;1(1):2.

17. M. Jarcho, J. F. Kay, K. I. Gumaer, R. H. Doremus, H. P. Drobeck. Tissue, cellular and subcellular events at a bone-ceramic hydroxylapatite interface. J Bioeng. 1977 Jan;1(2):79–92.

18. Brown S, Clarke I, Williams P, editors. Bioceramics. Switzerland: Trans Tech Pubn; 2002. 704 p.

19. Maurilio Marcacci, Elizaveta Kon, Vladimir Moukhachev, Andrei Lavroukov, Sergej Kutepov, Rodolfo Quarto, et al. Stem cells associated with macroporous bioceramics for long bone repair: 6- to 7-year outcome of a pilot clinical study. Tissue Eng. 2007 May;13(5):947–55.

20. Robert Lanza, Robert Langer, Joseph P. Vacanti, editors. Principles of Tissue Engineering, 4th Edition. 4 edition. Amsterdam: Academic Press; 2013. 1936 p.

21. Keith T. Paige, Linda G. Cima, Michael J. Yaremchuk, Joseph P. Vacanti, Charles A. Vacanti. Injectable Cartilage. Plast Reconstr Surg. 1995;96:1390.

22. Davide Campoccia, Patrick Doherty, Marco Radice, Paola Brun, Giovanni Abatangelo, David F. Williams. Semisynthetic resorbable materials from hyaluronan esterification. Biomaterials. 1998 Dec;19(23):2101–27.

23. Aldo R. Boccaccini, Veronique Maquet. Bioresorbable and bioactive polymer/Bioglass® composites with tailored pore structure for tissue engineering applications. Compos Sci Technol. 2003;63(16):2417–29.

24. Rezwan K, Chen QZ, Blaker JJ, Boccaccini AR. Biodegradable and bioactive porous polymer/inorganic composite scaffolds for bone tissue engineering. Biomaterials. 2006 Jun;27(18):3413–31.

25. Murphy CM, Haugh MG, O'Brien FJ. The effect of mean pore size on cell attachment, proliferation and migration in collagen–glycosaminoglycan scaffolds for bone tissue engineering. Biomaterials. 2010 Jan;31(3):461–6.

26. Peter X. Ma, Ruiyun Zhang, Guozhi Xiao, Renny Franceschi. Engineering new bone tissue in vitro on highly porous poly(α-hydroxyl acids)/hydroxyapatite composite scaffolds. J Biomed Mater Res. 2001;54(2):284–93.

27. Liu X, Ma PX. Polymeric Scaffolds for Bone Tissue Engineering. Ann Biomed Eng. 2004 Mar;32(3):477–86.

28. Ma PX, Zhang R. Synthetic nano-scale fibrous extracellular matrix. J Biomed Mater Res. 1999;46(1):60–72.

29. Horii A, Wang X, Gelain F, Zhang S. Biological Designer Self-Assembling Peptide Nanofiber Scaffolds Significantly Enhance Osteoblast Proliferation, Differentiation and 3-D Migration. PLoS ONE [Internet]. 2007 Feb 7 [cited 2015 Feb 23];2(2). Available from: http://www.ncbi.nlm.nih.gov/pmc/articles/PMC1784071/

30. Huang Z-M, Zhang Y-Z, Kotaki M, Ramakrishna S. A review on polymer nanofibers by electrospinning and their applications in nanocomposites. Compos Sci Technol. 2003 Nov;63(15):2223–53.

31. Sachlos E, Czernuszka JT. Making tissue engineering scaffolds work. Review: the application of solid freeform fabrication technology to the production of tissue engineering scaffolds. Eur Cell Mater. 2003 Jun 30;5:29–39; discussion 39–40.

32. Nam YS, Park TG. Biodegradable polymeric microcellular foams by modified thermally induced phase separation method. Biomaterials. 1999 Oct;20(19):1783–90.

33. Petka WA, Harden JL, McGrath KP, Wirtz D, Tirrell DA. Reversible Hydrogels from Self-Assembling Artificial Proteins. Science. 1998 Jul 1;281:389.

34. Tucker. The History of the Science and Technology of Electrospinning from 1600 to 1995. 2012;7:63–73.

35. Sakina R, Ali M. An Appraisal of the Efficacy and Effectiveness of Nanoscaffolds Developed by Different Techniques for Bone Tissue Engineering Applications: Electrospinning A Paradigm Shift. Adv Polym Technol. 2014;33(4):n/a – n/a.

36. Li D, Xia Y. Electrospinning of Nanofibers: Reinventing the Wheel? Adv Mater. 2004;16(14):1151–70.

37. Frenot A, Chronakis IS. Polymer nanofibers assembled by electrospinning. Curr Opin Colloid Interface Sci. 2003 Mar;8(1):64–75.

38. Zhang YZ, Su B, Venugopal J, Ramakrishna S, Lim CT. Biomimetic and bioactive nanofibrous scaffolds from electrospun composite nanofibers. Int J Nanomedicine. 2007;2(4):623–38.

39. Reneker DH, Yarin AL, Fong H, Koombhongse S. Bending instability of electrically charged liquid jets of polymer solutions in electrospinning. J Appl Phys. 2000 May 1;87(9):4531–47.

40. Demir MM, Yilgor I, Yilgor E, Erman B. Electrospinning of polyurethane fibers. Polymer. 2002 May;43(11):3303–9.

41. Maribel I. Baker, Steven P. Walsh, Zvi Schwartz, Barbara D. Boyan. A review of polyvinyl alcohol and its uses in cartilage and orthopedic applications. J Biomed Mater Res B Appl Biomater. 2012;100B(5):1451–7.

42. Tubbs RK. Sequence distribution of partially hydrolyzed poly(vinyl acetate). J Polym Sci [A1]. 1966;4(3):623–9.

43. Covey AM, Tuorto S, Brody LA, Sofocleous CT, Schubert J, von Tengg-Kobligk H, et al. Safety and efficacy of preoperative portal vein embolization with polyvinyl alcohol in 58 patients with liver metastases. AJR Am J Roentgenol. 2005 Dec;185(6):1620–6.

44. Maquet V, Martin D, Malgrange B, Franzen R, Schoenen J, Moonen G, et al. Peripheral nerve regeneration using bioresorbable macroporous polylactide scaffolds. J Biomed Mater Res. 2000 Dec 15;52(4):639–51.

45. Weis C, Odermatt EK, Kressler J, Funke Z, Wehner T, Freytag D. Poly(vinyl alcohol) membranes for adhesion prevention. J Biomed Mater Res B Appl Biomater. 2004 Aug 15;70(2):191–202.

46. Bray JC, Merrill EW. Poly(vinyl alcohol) hydrogels for synthetic articular cartilage material. J Biomed Mater Res. 1973;7(5):431–43.

47. Kempson GE, Muir H, Pollard C, Tuke M. The tensile properties of the cartilage of human femoral condyles related to the content of collagen and glycosaminoglycans. Biochim Biophys Acta BBA - Gen Subj. 1973 Feb 28;297(2):456–72.

48. Almarza AJ, Athanasiou KA. Design Characteristics for the Tissue Engineering of Cartilaginous Tissues. Ann Biomed Eng. 2004 Jan 1;32(1):2–17.

49. Jason A. Stammen, Stephen Williams, David N. Ku, Robert E. Guldberg. Mechanical properties of a novel PVA hydrogel in shear and unconfined compression. Biomaterials. 2001 Apr;22(8):799–806.

50. Holloway JL, Spiller KL, Lowman AM, Palmese GR. Analysis of the in vitro swelling behavior of poly(vinyl alcohol) hydrogels in osmotic pressure solution for soft tissue replacement. Acta Biomater. 2011 Jun;7(6):2477–82.

51. Chahal S, Hussain FSJ, Yusoff MBM. Characterization of Modified Cellulose (MC)/Poly (Vinyl Alcohol) Electrospun Nanofibers for Bone Tissue Engineering. Procedia Eng. 2013;53:683–8.

52. Kim G-M, Asran AS, Michler GH, Simon P, Kim J-S. Electrospun PVA/HAp nanocomposite nanofibers: biomimetics of mineralized hard tissues at a lower level of complexity. Bioinspir Biomim. 2008 Dec 1;3(4):046003.

53. Spicer PP, Kretlow JD, Young S, Jansen JA, Kasper FK, Mikos AG. Evaluation of bone regeneration using the rat critical size calvarial defect. Nat Protoc. 2012 Sep 27;7(10):1918–29.

54. Salgado AJ, Coutinho OP, Reis RL. Bone tissue engineering: state of the art and future trends. Macromol Biosci. 2004 Aug 9;4(8):743–65.

55. Yang Y, Wimpenny I, Ahearne M. Portable nanofiber meshes dictate cell orientation throughout three-dimensional hydrogels. Nanomedicine Nanotechnol Biol Med. 2011 Apr;7(2):131–6.

56. Vaquette C, Cooper-White J. A simple method for fabricating 3-D multilayered composite scaffolds. Acta Biomater. 2013 Jan;9(1):4599–608.

57. Leung LH, Fan S, Naguib HE. Fabrication of 3D electrospun structures from poly(lactide-co-glycolide acid)–nano-hydroxyapatite composites. J Polym Sci Part B Polym Phys. 2012;50(4):242–9.

58. Madurantakam PA, Rodriguez IA, Garg K, McCool JM, Moon PC, Bowlin GL. Compression of Multilayered Composite Electrospun Scaffolds: A Novel Strategy to Rapidly Enhance Mechanical Properties and Three Dimensionality of Bone Scaffolds. Adv Mater Sci Eng. 2013 Jan 13;2013:e561273.

59. Woodfield TBF, Malda J, de Wijn J, Péters F, Riesle J, van Blitterswijk CA. Design of porous scaffolds for cartilage tissue engineering using a three-dimensional fiber-deposition technique. Biomaterials. 2004 Aug;25(18):4149–61.

60. Park SA, Kim HJ, Lee SH, Lee JH, Kim HK, Yoon TR, et al. Fabrication of nano/microfiber scaffolds using a combination of rapid prototyping and electrospinning systems. Polym Eng Sci. 2011 Sep 1;51(9):1883–90.

61. Drobnič M, Radosavljevič D, Ravnik D, Pavlovčič V, Hribernik M. Comparison of four techniques for the fixation of a collagen scaffold in the human cadaveric knee. Osteoarthritis Cartilage. 2006 Apr 1;14(4):337–44.

62. Dell'Accio F, Vanlauwe J, Bellemans J, Neys J, De Bari C, Luyten FP. Expanded phenotypically stable chondrocytes persist in the repair tissue and contribute to cartilage matrix formation and structural integration in a goat model of autologous chondrocyte implantation. J Orthop Res. 2003;21(1):123–31.

63. Deitzel J, Kleinmeyer J, Harris D, Tan NB. The effect of processing variables on the morphology of electrospun nanofibers and textiles. Polymer. 2001;42(1):261–72.

64. Yang Q, Li Z, Hong Y, Zhao Y, Qiu S, Wang C, et al. Influence of solvents on the formation of ultrathin uniform poly(vinyl pyrrolidone) nanofibers with electrospinning. J Polym Sci Part B Polym Phys. 2004 Oct 15;42(20):3721–6.

65. Karageorgiou V, Kaplan D. Porosity of 3D biomaterial scaffolds and osteogenesis. Biomaterials. 2005 Sep;26(27):5474–91.